Cell Reports

Article

The C5a-C5aR1 complement axis is essential for neutrophil recruitment to draining lymph nodes via high endothelial venules in cutaneous leishmaniasis

Graphical abstract

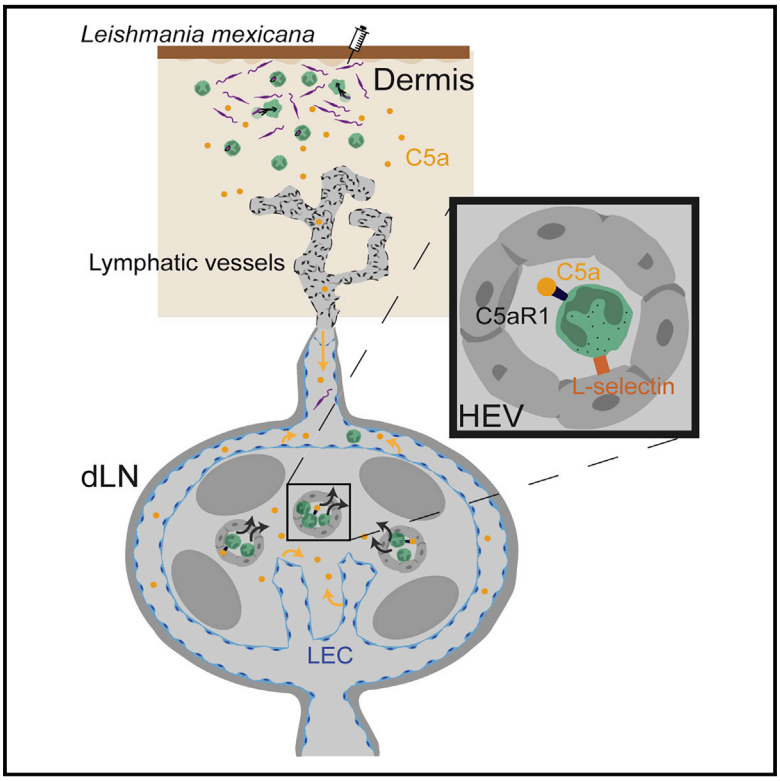

Highlights

- Neutrophils enter dLNs mainly via high endothelial venules
- The C5a-C5aR1 complement axis is involved in their recruitment to the dLNs
- C5 is produced locally in the dLNs by lymphatic endothelial cells
- L-Selectin is fundamental for neutrophil recruitment

Authors

Borja Prat-Luri, Christopher Neal, Katiuska Passelli, ..., Tatiana V. Petrova, Andreas J. Müller, Fabienne Tacchini-Cottier

Correspondence

borja.pratluri@unil.ch (B.P.-L.), fabienne.tacchini-cottier@unil.ch (F.T.-C.)

In brief

Prat-Luri et al. characterize the mechanisms involved in neutrophil recruitment to the draining lymph node following dermal infection with *Leishmania mexicana* parasites. Neutrophil recruitment occurred predominantly via high endothelial venules, a process mediated by the C5a-C5aR1 axis. C5/C5a are locally produced by lymphatic endothelial cells in the draining lymph node.

Prat-Luri et al., 2022, Cell Reports *39*, 110777
May 3, 2022
https://doi.org/10.1016/j.celrep.2022.110777

CellPress

Cell Reports

CellPress
OPEN ACCESS

Article

The C5a-C5aR1 complement axis is essential for neutrophil recruitment to draining lymph nodes via high endothelial venules in cutaneous leishmaniasis

Borja Prat-Luri,[1,*] Christopher Neal,[1] Katiuska Passelli,[1] Emma Ganga,[1] Jonas Amore,[2] Luan Firmino-Cruz,[1,5] Tatiana V. Petrova,[3,4] Andreas J. Müller,[2] and Fabienne Tacchini-Cottier[1,6,*]

[1]Department of Immunobiology, WHO Collaborative Center for Research and Training in Immunology, University of Lausanne, Epalinges, Switzerland

[2]Otto-von-Guericke-University Magdeburg and Helmholtz Centre for Infection Research Braunschweig, Magdeburg, Germany

[3]Department of Oncology, University of Lausanne, Epalinges, Switzerland

[4]Ludwig Institute for Cancer Research Lausanne, Epalinges, Switzerland

[5]Present address: Instituto de Microbiologia Paulo de Góes, Laboratório de Imunobiotecnologia, Universidade Federal do Rio de Janeiro, Rio de Janeiro-RJ, Brazil

[6]Lead contact

*Correspondence: borja.pratluri@unil.ch (B.P.-L.), fabienne.tacchini-cottier@unil.ch (F.T.-C.)

https://doi.org/10.1016/j.celrep.2022.110777

SUMMARY

Neutrophils are specialized innate immune cells known for their ability to fight pathogens. However, the mechanisms of neutrophil trafficking to lymph nodes are not fully clear. Using a murine model of dermal infection with *Leishmania* parasites, we observe a transient neutrophil influx in draining lymph nodes despite sustained recruitment to the infection site. Cell-tracking experiments, together with intravital two-photon microscopy, indicate that neutrophil recruitment to draining lymph nodes occurs minimally through lymphatics from the infected dermis, but mostly through blood vessels via high endothelial venules. Mechanistically, neutrophils do not respond to IL-1β or macrophage-derived molecules. Instead, they are guided by the C5a-C5aR1 axis, using L-selectin and integrins, to extravasate into the draining lymph node parenchyma. We also report that C5, the C5a precursor, is locally produced in the draining lymph node by lymphatic endothelial cells. Our data establish and detail organ-specific mechanisms of neutrophil trafficking.

INTRODUCTION

Neutrophils have long been recognized as part of the front-line defense against infections. Indeed, neutrophils can kill pathogens, such as bacteria and parasites, with a plethora of different mechanisms. These include phagocytosis, the release of preformed granules that contain lytic enzymes, and the induction of oxidative burst. In addition, neutrophils are also able to release web-like structures composed of DNA associated with protein granules, a process termed neutrophil extracellular trap formation that can kill trapped pathogens (Burn et al., 2021).

In recent years, neutrophils have been shown to also contribute to the regulation of the adaptive immunity (Leliefeld et al., 2015). They produce cytokines that can affect the development of the developing immune response (Tecchio and Cassatella, 2016). Moreover, neutrophils can increase or suppress T cell responses through several mechanisms, including their release of arginase 1 or ROS production (Aarts et al., 2019; Beauvillain et al., 2007; Didelija et al., 2017; Yang and Unanue, 2013). Similarly, neutrophils were also reported to display this dual role for B cells by either promoting or limiting the production of antigen-specific antibodies (Kamenyeva et al., 2015; Parsa et al., 2016; Puga et al., 2011).

Both human and murine lymph nodes harbor few neutrophils under homeostatic conditions (Bogoslowski et al., 2020; Casanova-Acebes et al., 2018; Lok et al., 2019). Following an insult, migration of neutrophils to draining lymph nodes (dLNs) has been reported, yet the mechanisms involved are not consistent among the different experimental models (Abadie et al., 2005; Bogoslowski et al., 2018; Chtanova et al., 2008; Hampton et al., 2015; Hampton and Chtanova, 2019; Rigby et al., 2015; Tacchini-Cottier et al., 2000). In response to *S. aureus* infection, neutrophils were suggested to predominantly reach the lymph node through lymphatic vessels (Hampton et al., 2015), while other reports showed their trafficking through blood vessels via high endothelial venules (HEVs) (Bogoslowski et al., 2018; Kamenyeva et al., 2015). Therefore, it is important to understand and characterize how neutrophils traffic and reach these secondary lymphoid organs in the context of different stimuli. Little is known about neutrophil trafficking into dLNs in response to cutaneous intracellular pathogens. We previously showed that neutrophils play a deleterious role during infections with the protozoan *Leishmania mexicana* parasite, allowing transient parasite survival in these cells and limiting the development of a Th1 response (Hurrell et al., 2015, 2017).

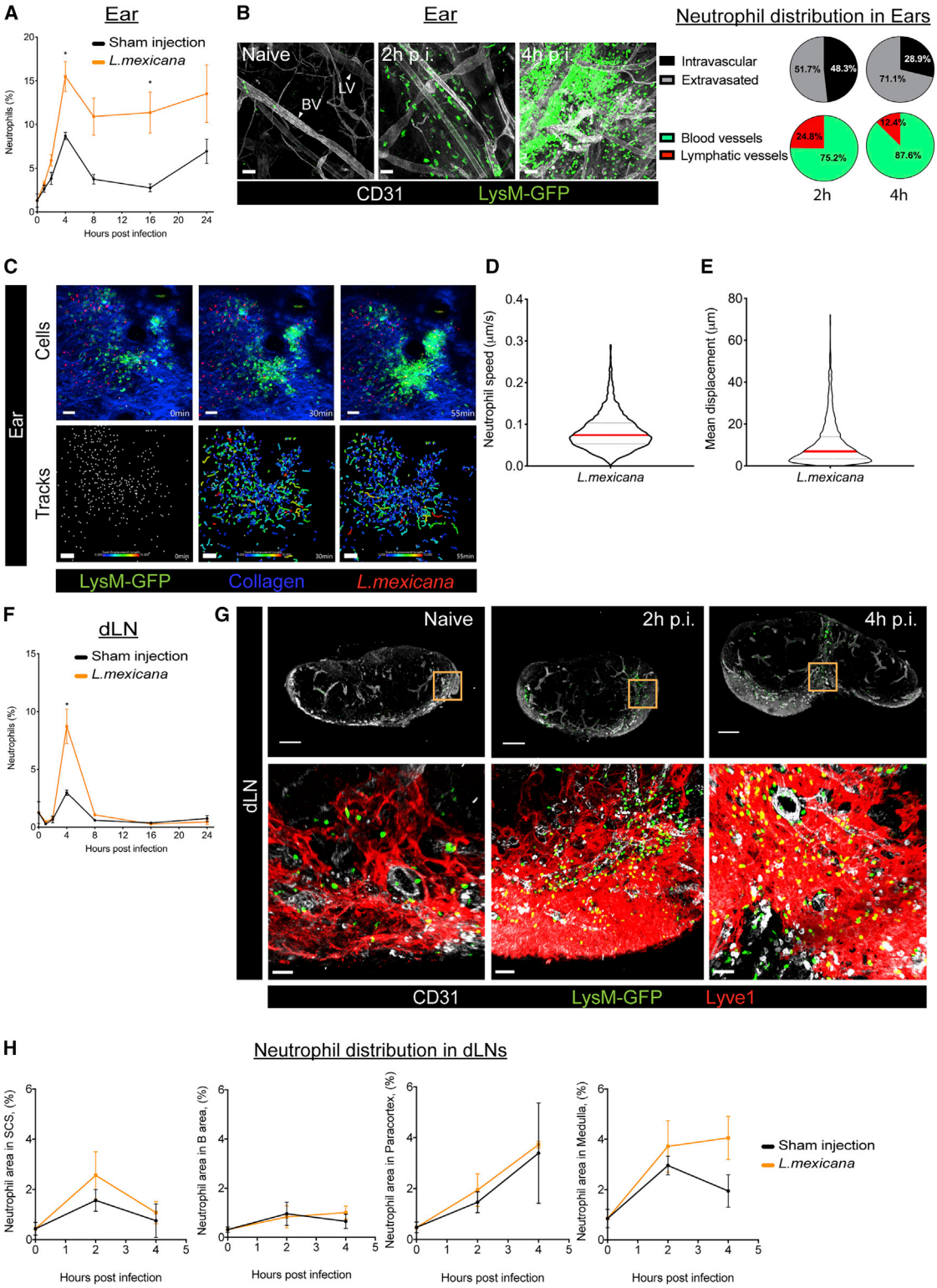

Figure 1. Neutrophil trafficking during early stages of *L. mexicana* infection

(A) Flow cytometry kinetic analysis of the frequency of recruited CD11b^{+}Ly6G^{+} neutrophils in the ear after infection with *L. mexicana* metacyclic parasites or with sham control.

(B) Left panel: representative whole-mount images of naive and infected ears 2 and 4 h p.i. stained for CD31^{+} (white) vessels and with LysM-GFP (green) neutrophils. BV, blood vessel; LV, lymphatic vessel. Scale bar, 30 μm. Right panel: pie chart quantification of neutrophil distribution in the ear parenchyma 2 and 4 h

(legend continued on next page)

Here, using this well-defined *L. mexicana* model, we investigated the kinetics and the mechanisms involved in neutrophil trafficking to dLNs after infection. Following intradermal infection, we show that a transient peak of neutrophils is observed in dLNs, although significantly less pronounced than that observed after infection with *S. aureus*. In response to *L. mexicana* infection, neutrophils were recruited from the bloodstream via HEVs. Their migration depended on the anaphylatoxin C5a, integrins, and L-selectin. In addition, this recruitment occurred independently of IL-1β secretion or LN macrophages. Our data show that the extent of neutrophil recruitment to dLNs is specifically adapted to the pathogenic threat, highlighting the differential molecular basis of their response according to the specific insult.

RESULTS

Neutrophil kinetics and localization at the infection site and dLNs at the onset of *L. mexicana* infection

To understand the trafficking of neutrophils to dLNs we first established the kinetic and distribution of these cells from a systemic point of view. To do so, the frequency of $CD11b^+Ly6G^+$ neutrophils was analyzed by flow cytometry in the blood, ear, and dLNs (Figure S1A) over the first 24 h following intradermal ear injection of metacyclic *L. mexicana* parasites into C57BL/6 mice. A rapid neutrophil release was observed in peripheral blood rising to a peak frequency of 50% of the $CD11b^+$ population 2–4 h after challenge and decreasing to steady-state levels 8 h p.i (Figure S1B). At the site of infection, the frequency of recruited neutrophils rose steadily during the first hours, reaching 15% of the myeloid population at 4 h p.i. and remaining around such level until 24 h p.i. (Figure 1A). Using whole-mount imaging, we visualized only few circulating neutrophils inside blood vessels in naive ears. Two hours post *L. mexicana* infection, up to 52% of all newly recruited neutrophils already extravasated the blood vasculature, reaching a frequency of about 70% at 4 h p.i. (Figure 1B). Once extravasated, the swarming behavior of these cells toward the parasite was observed by two-photon intravital microscopy (2P-IVM) with a mean speed of 0.07 μm/s and a mean displacement of 10.6 μm (Figures 1C and 1D–1E; Video S1). Of note, most intravascular neutrophils were found inside the blood vascular network, with only between one-fourth to one-eighth of the neutrophils detected within the lymphatic vessels at 2 and 4 h p.i., respectively (Figure 1B).

In the dLNs, a transient peak of neutrophils was observed by flow cytometry at 4 h p.i., reaching 9% of the $CD11b^+$ myeloid population (Figure 1F). Using immunofluorescence staining in tiled dLN images of infected LysM-GFP knockin mice, we detected neutrophils already in steady-state conditions (Figure 1G), in line with recent reports (Bogoslowski et al., 2020; Casanova-Acebes et al., 2018; Lok et al., 2019). Spatially, the neutrophil distribution in the dLNs differed in the areas of the LNs: we observed a transient increase in the subcapsular sinus (SCS) 2 h p.i., while in the medulla this remained constant until 4 h p.i (Figures 1G and 1H). Of note, neutrophil frequency in the bone marrow and in inguinal non-draining LNs were unchanged 4 h p.i. infection. However, an increased frequency of neutrophils was observed in the spleen, as reported in other models (Deniset et al., 2017) (Figure S1C).

To screen for the presence of parasites in dLNs, we injected a transgenic dsRed-expressing *L. mexicana* strain. Histologic analysis revealed that parasites were present in 70% of the dLNs analyzed 2 h post infection, mostly restrained to the SCS (Figures S2A and S2B). Four hours post infection a limited amount of parasites was detected in 33% of dLNs (Figure S2C).

In summary, at the onset of *L. mexicana* infection, a neutrophilic response is induced and sustained in the ear, while in the dLNs there is a transient neutrophil influx that predominates in the medulla.

A minor proportion of neutrophils present in the dLNs come from the infected site

To compare the neutrophilic response against *L. mexicana* with other pathogens known to attract neutrophils in the dLNs (Hampton et al., 2015), we injected in the ear dermis *S. aureus* bioparticles. Both bacteria and parasites induced recruitment of neutrophils into the injected ear, as detected by whole-mount staining (Figure 2A). Furthermore, *S. aureus* bioparticles induced a more significant neutrophilic response in comparison to *L. mexicana*, as assessed by flow cytometry (Figure 2B). This difference was even more pronounced in the auricular dLNs, as visualized by whole-mount staining (Figure 2C) and quantified by flow cytometry (Figure 2D). We next sought to understand whether this increase in neutrophils at the dLNs was due to an increased migration of neutrophils from the infection site. To this end, we used Kikume mice that express the KikGR fluorescent photoconvertible protein, allowing cell tracking across the

p.i. showing the frequency of intravascular (black) or extravasated (gray) neutrophils. Pie chart of intravascular neutrophils shows the frequency of neutrophils found in blood (green) or lymphatic vessels (red).

(C) Upper panel: representative 2P-IVM images of neutrophils (LysM-GFP, green) swarming toward *L. mexicana* (dsRed, red) metacyclic promastigotes in the ear dermis 2 h p.i. Collagen fibers are shown in blue. Scale bar, 30 μm. Bottom panel: tracks generated by neutrophils during the recording time. Color coded is shown the displacement length of the track. Scale bar, 30 μm.

(D and E) Quantification of 2P-IVM imaging data from (C) showing (D). Neutrophil track speed (μm/s) and (E). Neutrophil mean track displacement (μm).

(F) Flow cytometry kinetic analysis of the frequency of recruited $CD11b^+Ly6G^+$ neutrophils in the dLNs after infection with *L. mexicana* metacyclic parasites or sham control.

(G) Upper panel: representative vibratome tiled sections of naive and infected dLNs 2 and 4 h p.i. Staining for CD31 (white) and LysM-GFP (green). Scale bar, 300 μm. Bottom panel: high-magnification images of the area outlined in the orange box in the upper panel. CD31 (white), Lyve1 (red), and LysM-GFP (green). Scale bar, 40 μm.

(H) Quantification of neutrophil distribution in dLN compartments over time. Data in (A) and (F) are representative of several independent experiments, where each time point was repeated at least two times with at least n = 3/time point and analyzed using a mixed-effect analysis with Sydak's multiple comparison test. *$p < 0.05$. Data in (B), (G), and (H) are from two independent experiments, each including n = 4–5/group. Data in (C), (D), and (E) are from two independent experiments.

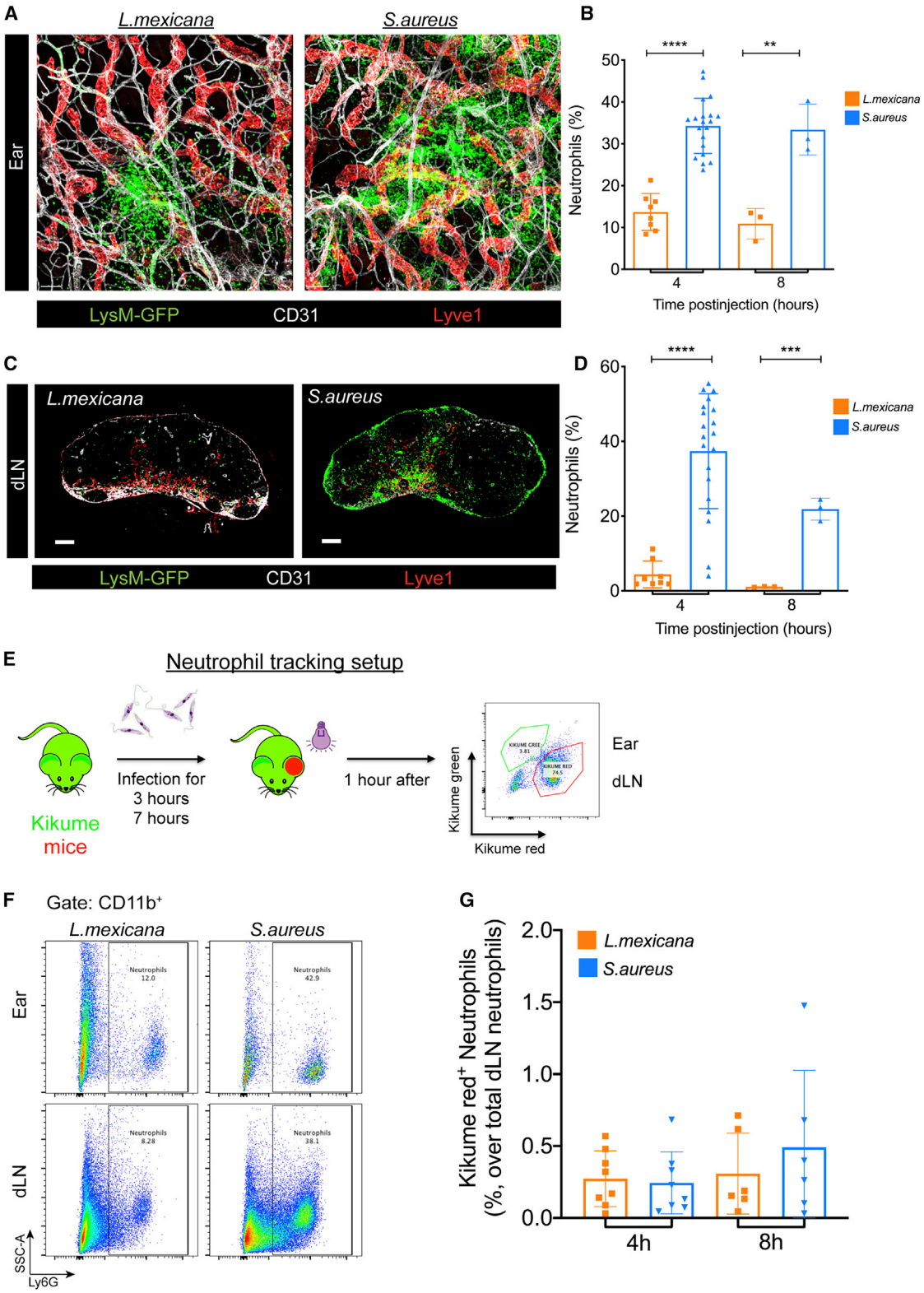

Figure 2. A minor proportion of neutrophils in the dLNs come from the infected dermis

(A) Representative whole-mount images of infected ears with either *L. mexicana* or *S. aureus* bioparticles 4 h p.i. Staining for CD31 (white), Lyve1 (red), and LysM-GFP (green). Scale bar, 50 μm.

(legend continued on next page)

organism (Heyde et al., 2018; Nowotschin and Hadjantonakis, 2009). Kikume mice were injected with *L. mexicana* or *S. aureus*, and 3 or 7 h later the infected ear was photoconverted from green to red and the dLNs were analyzed 1 h later (Figures 2E and S2A). The frequency of recruited neutrophils in the ear and dLNs was in accordance with what we previously observed after infection of C57BL/6 mice (Figure 2F). To further characterize the cells egressing from the site of infection, we analyzed the frequency of $CD11b^{+}Ly6G^{+}$ Kikume red-positive cells that had been photoconverted in the ear using flow cytometry. Using the two different time points after infection, we observed that less than 0.5% of the neutrophil population present in the dLNs was positive for Kikume red and thus coming from the infection site (Figure 2G). Furthermore, using a transendothelial *in vitro* migration assay, we observed that, upon *L. mexicana* infection, neutrophils were less able to transmigrate through a lymphatic endothelial monolayer. Even more, infected neutrophils were less able to migrate in response to CXCL1 (KC), suggesting that infection by the parasite impairs neutrophil migration (Figure S2B).

Collectively, our data indicate that the neutrophil influx observed at the dLNs after *L. mexicana* or *S. aureus* bioparticle injection is, in its major part, a recruitment to the dLNs rather than a migration from the infected dermis.

Neutrophil trafficking to the dLNs happens mostly through the bloodstream via HEV in response to *L. mexicana* dermal infection

Our previous data suggested that the migration of neutrophils from the infection site to the dLNs through lymphatic vessels is minimal. To confirm this and visualize the process, we generated Prox1-mOrange/LysM-GFP bone marrow chimeras (Figure 3A). These chimeras express GFP^{high} neutrophils and mOrange lymphatics, allowing the tracking of neutrophils in lymphatic vessels. As a proof of concept, we used the footpad model and corresponding draining popliteal LNs for our 2P-IVM LN studies, due to technical limitations precluding 2P-IVM on auricular LNs. We first corroborated by flow cytometry that, in this LN, neutrophil recruitment was observed 4 h p.i (Figure S3C). We also assessed the effect of the procedure itself on neutrophil recruitment and observed that very few neutrophils were present in naive or vehicle-injected dLNs (Figure S4A; Video S2). Following s.c. infection of *L. mexicana*, neutrophils were observed in the dLNs 30 min p.i., already swarming after 75 min (Figure 3B; Video S3) with a mean speed of 0.16 μm/s (Figure 3C). However, very few neutrophils were found in lymphatic vessels. Indeed, only 1.4% of neutrophils observed were interacting with such vessel (Figure 3D) and most of them were far away throughout the recording time, indicating that neutrophils do not migrate through lymphatic vessels. In addition, ear 2P-IVM also revealed that most neutrophils at the infection site were not or very transiently interacting with such vessels (Figure S4B; Video S4). Ear whole-mount staining corroborated these findings and showed that the frequency of neutrophils inside the capillary or collecting lymphatic vascular beds was 7% or 4%, respectively (Figures S4C and S4D).

We next performed 2P-IVM on dLNs after infection using MECA-79 i.v. labeling to visualize HEVs, as these specialized blood vessels are known to be the site of leukocyte extravasation into dLNs (Bai et al., 2013; Blanchard and Girard, 2021; Brulois et al., 2020). We observed approximately 40% of the neutrophils entering the organ by means of HEVs (Figures 3E and 3F;Video S5), with a mean speed of 0.13 μm/s (Figure 3G).

Altogether, these results establish that neutrophils in response to *L. mexicana* dermal infection are mostly recruited from the bloodstream through HEVs into the dLNs.

L-Selectin is essential for neutrophil extravasation into the dLN parenchyma in response to *L. mexicana* dermal infection

We next investigated the ligands used by neutrophils to engage on the endothelium to eventually be able to cross and extravasate into the dLNs. Among those, selectins, such as L-selectin and PSGL-1, are the first molecules used by neutrophils in this process (Hyun and Hong, 2017; Kolaczkowska and Kubes, 2013). To study their involvement in neutrophil trafficking in response to *L. mexicana* infection, we administered blocking antibodies against these selectins i.v. 1 h before infection (Figure 4A). Depletion of L-selectin alone resulted in a significant reduction of neutrophils recruited to the dLNs (Figure 4B). The treatment also reduced the number of neutrophils observed at the infection site and peripheral blood (Figures 4C, S5A, and S5B). Blockade of PSGL-1 resulted in a similar effect to L-selectin blockade at the infection site (Figure 4D). Nonetheless, in the dLN neutrophils were not impacted by PSGL-1 blockade, highlighting organ-specific differences (Figure 4B). Depletion of both L-selectin and PSGL-1 resulted in a synergistic effect in the ear (Figure 4C) and recapitulated the L-selectin effect in the draining LNs (Figure 4B).

Once neutrophils engage the endothelium by means of selectins, integrins come next to form more stable and stronger interactions (Schnoor et al., 2021). To investigate the importance of integrins in neutrophil recruitment, we blocked LFA-1, Mac-1, or VLA4, or all three together before infection, and analyzed the influx of neutrophils in the dLNs. LFA-1 blockade resulted in a decrease of neutrophils at the infection site (Figure 4E), but no

(B) Flow cytometry analysis of the frequency of $CD11b^{+}Ly6G^{+}$ neutrophils in the ear dermis 4 and 8 h p.i. with *L. mexicana* or *S. aureus* bioparticles.
(C) Representative cryosection tiled images of dLNs 4 h after i.d. injection of *L. mexicana* or *S. aureus* bioparticles. Staining for CD31 (white), Lyve1 (red), and LysM-GFP (green). Scale bar, 200 μm.
(D) Flow cytometry analysis of $CD11b^{+}Ly6G^{+}$ neutrophils in dLNs 4 and 8 h p.i. after *L. mexicana* or *S. aureus* bioparticles infection.
(E) Experimental strategy for neutrophil tracking experiments from the site of infection to the dLNs.
(F) Representative flow cytometry plots showing the frequency of neutrophils in the ear and dLNs of Kikume mice 4 h p.i.
(G) Quantification of the fraction of photoconverted (PC) neutrophils as compared with total neutrophil in the dLNs. Data in (B) and (D) are pooled from three independent experiments, with at least n = 3/group. Data were analyzed using two-tailed unpaired Student's t test; $^{**}p < 0.01$, $^{***}p < 0.001$, $^{****}p < 0.0001$. Data in (G) are pooled from two independent experiments, with n = 4/group.

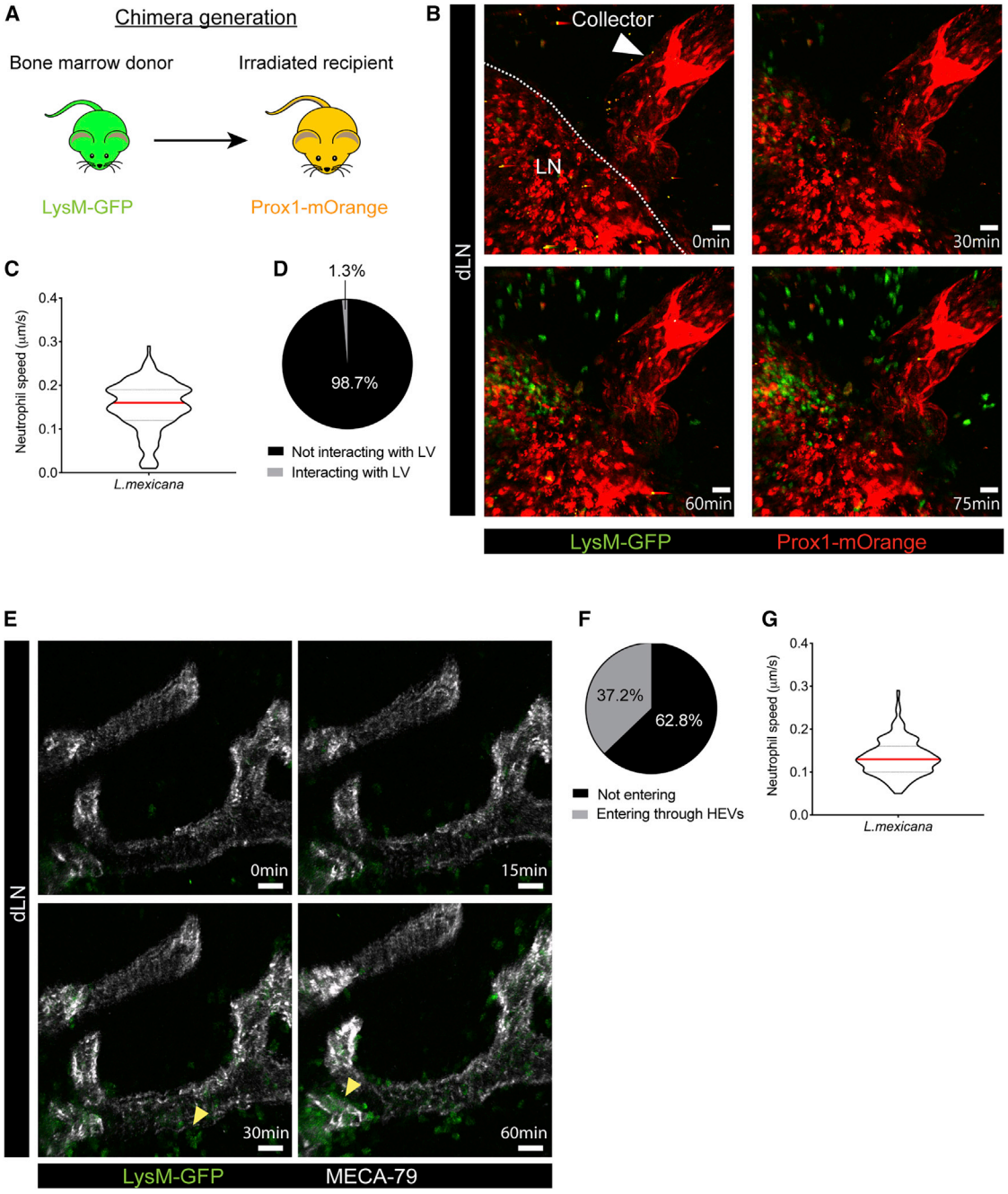

Figure 3. Most neutrophils arrive to the dLNs through the bloodstream via HEVs in response to *L. mexicana* dermal infection

(A) Experimental design used to generate the LysM-GFP/Prox1-mOrange BM chimeras.

(B) Snapshots from a representative intravital imaging movie of the dLNs of LysM-GFP/Prox1mOrange chimeras after *L. mexicana* s.c. infection, showing green neutrophils and red lymphatics. Scale bar, 30 μm.

(C) Analysis of the neutrophil speed (μm/s) in dLNs.

(D) Proportion of neutrophils interacting with collecting lymphatic vessels in the dLNs after infection.

(E) Representative snapshots from 2P-IVM of dLNs of LysM-GFP (green) mice that were injected i.v. with labeled MECA79 (white) antibody labeling HEVs, before s.c. infection with *L. mexicana*. Scale bar, 20 μm.

(F) Quantification of 2P-IVM imaging data from (E) showing the frequency of neutrophils entering or not through HEVs and (G). the neutrophil speed in the dLNs (μm/s). Data from (B), (C), and (D) are from three independent experiments, while data from (E), (F), and (G) are from two independent experiments.

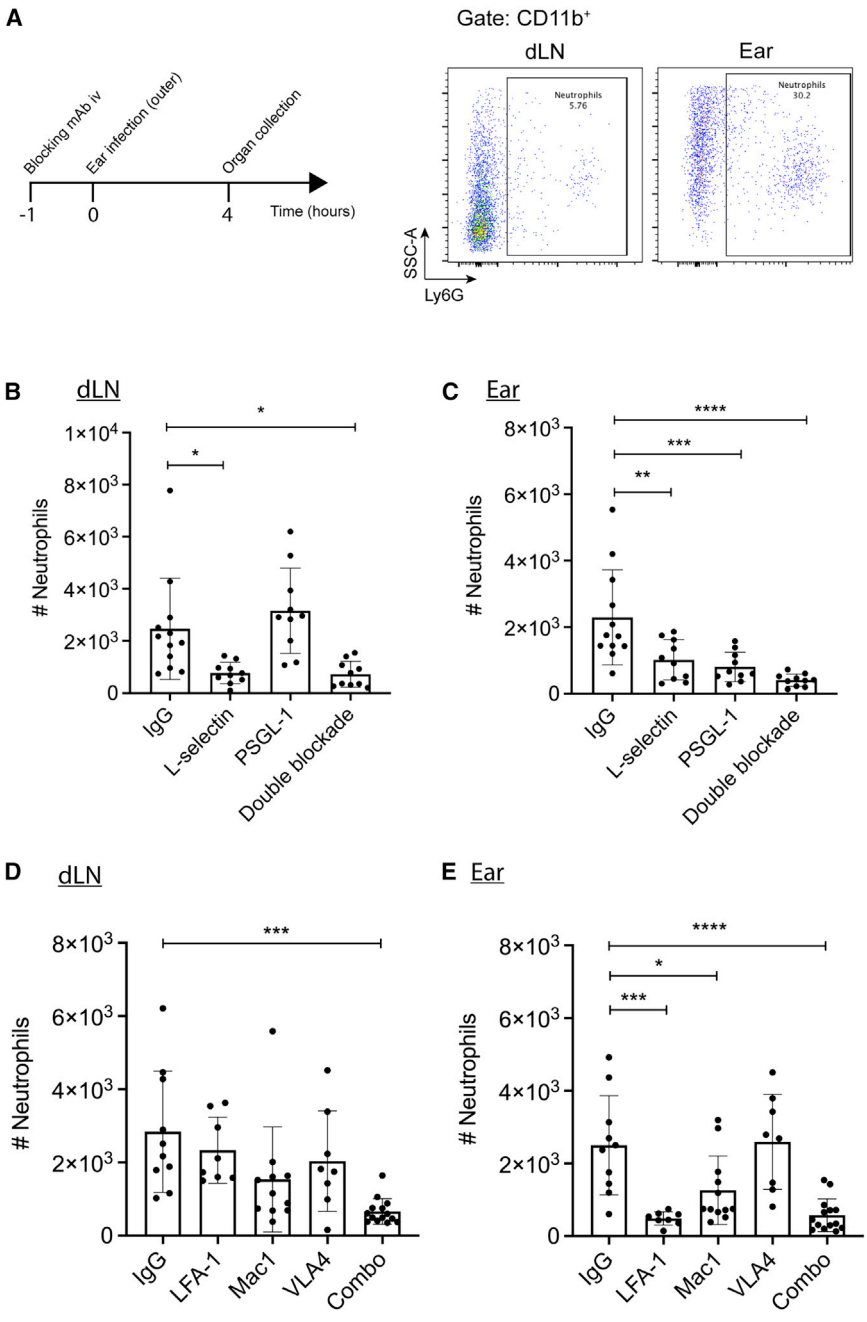

Figure 4. Neutrophil extravasation into the dLN parenchyma is integrin dependent and relies on L-selectin

(A) Experimental strategy for selectin and integrin blocking experiments. Representative flow cytometry plots showing the frequency of neutrophils in the dLNs and ear in the IgG isotype control.

(B) Quantification of neutrophil numbers in the dLNs 4 h after *L. mexicana* dermal infection upon the indicated selectin-blocking treatments.

(C) Quantification of neutrophil numbers in the ear 4 h after *L. mexicana* dermal infection upon the indicated selectin-blocking treatments.

(D) Quantification of neutrophil numbers in dLNs 4 h after *L. mexicana* dermal infection upon the indicated integrin-blocking treatments.

(E) Quantification of neutrophil numbers in ears 4 h after *L. mexicana* dermal infection upon the indicated integrin-blocking treatments. Data from (B), (C), (D), and (E) are from three independent experiments, with at least n = 3/group. Data were analyzed by one-way ANOVA with Dunnett's multiple comparison tests; *p < 0.05, **p < 0.01, ***p < 0.001, ****p < 0.0001.

difference was observed in the dLNs (Figure 4D). Similarly, Mac1 blockade resulted in a decrease of neutrophil numbers in the ear but not in the dLNs (Figures 4D and 4E). On the other hand, VLA4 blocking did not alter the influx of neutrophils to the dLNs or ear (Figures 4D and 4E). Of note, blockade of the three integrins led to a significant decrease of neutrophils recruited to both the dLNs and the ear (Figures 4D and 4E), suggesting that a compensatory mechanism might take place when performing single blockade. Blockade of Mac1 alone or the three integrins together led to an increased frequency of neutrophils in peripheral blood (Figures S5C and S5D).

Collectively, these data demonstrate organ-specific differences in the molecules utilized by neutrophils to extravasate. In the dLNs, L-selectin is essential for neutrophil recruitment; however, downstream molecules remain unidentified. In the skin we show that, in addition to L-selectin, neutrophils engage PSGL1, Mac1, and LFA-1 to carry out this process.

Early neutrophil recruitment to dLNs in response to *L. mexicana* infection is macrophage and IL-1β independent

Previous studies using bacterial and viral models had established that neutrophils are recruited to the dLNs via inflammasome-dependent mechanisms. Indeed, macrophage-derived IL-1β at the SCS was responsible for the recruitment of neutrophils (Kastenmuller et al., 2012). Therefore, we next explored whether neutrophils in response to *L. mexicana* would behave in a similar manner. We first performed immunofluorescence staining for pro and mature IL-1β in naive and dLNs from infected ears. In resting conditions, we detected IL-1β in the majority in macrophages, both in the SCS and the medulla. Four hours after *L. mexicana* infection, staining was especially prominent in SCS and medullary areas, where we observed colocalization with GFP^{high} neutrophils and $CD169^{+}$ macrophages (Figures 5A and 5B). Of note, we also detected IL-1β in other cell types, most likely dendritic cells and endothelial cells (Figure 5B), as observed in other studies (Brulois et al.,

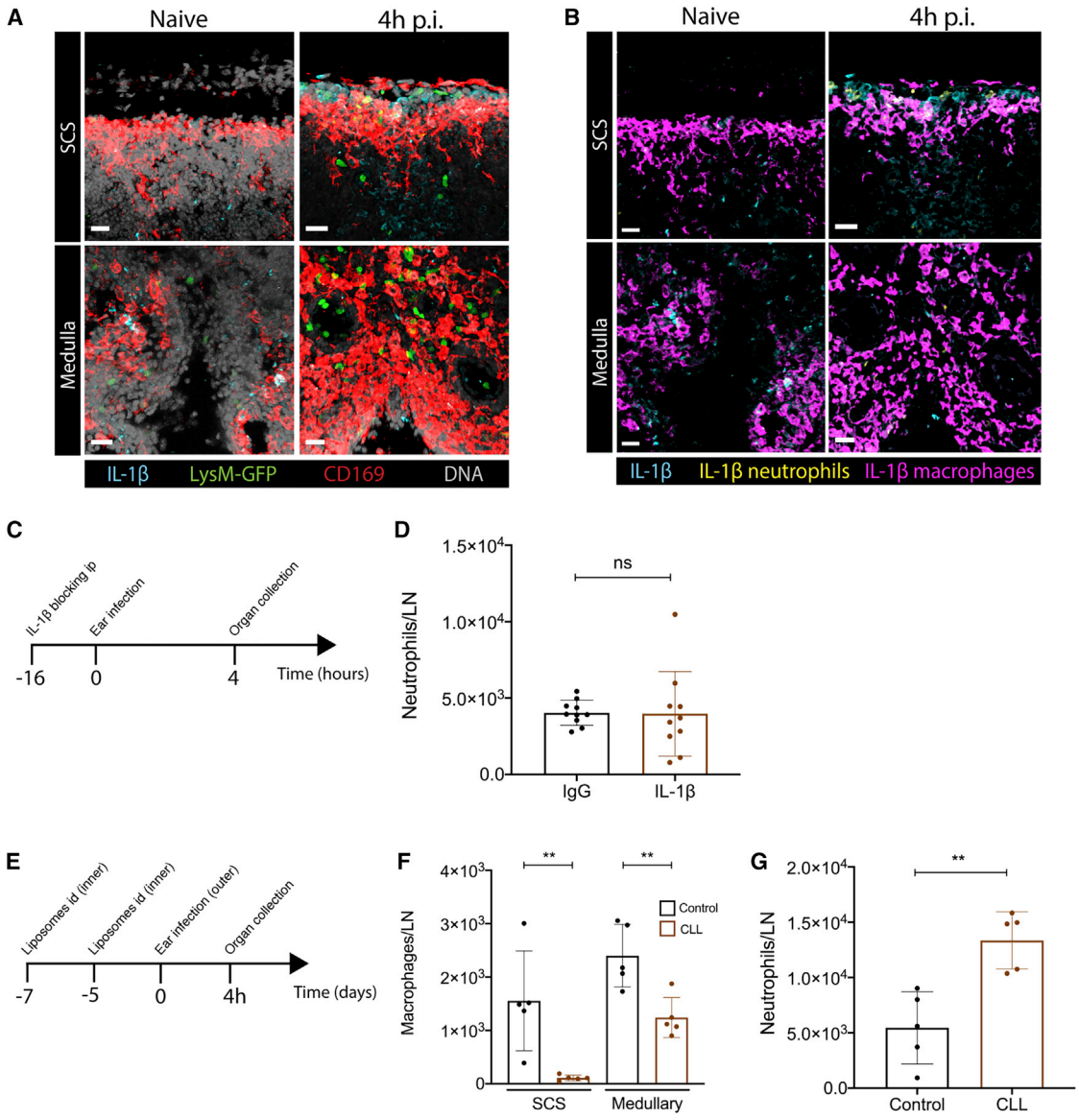

Figure 5. Neutrophil recruitment to dLNs in response to *L. mexicana* dermal infection is independent of IL-1β and dLN macrophages

IL-1β protein is deposited in the SCS (upper panels) and medulla (bottom panel) of naive and infected dLNs 4 h after *L. mexicana* i.d. infection. Staining for IL-1β (cyan), CD169 (red), LysM-GFP (green), and DNA (gray). Scale bar, 20 μm.

(B) IL-1β expression in macrophages (pink), neutrophils (yellow), or any other cell type (cyan) is shown following analysis with cell-specific masks.

(C) Experimental strategy for IL-1β blocking experiments.

(D) The number of $CD11b^+Ly6G^+$ dLN neutrophils was assessed by flow cytometry after IL-1β blocking or isotype IgG treatments.

(E) Experimental design for the macrophage depletion experiments.

(F) The efficiency of depletion was analyzed by flow cytometry of the dLN SCS ($CD169^+F4/80^-$) and medullary ($CD169^+F4/80^+$) macrophages.

(G) The number of $CD11b^+Ly6G^+$ dLN neutrophils was as assessed by flow cytometry after clodronate or control liposome treatment. Data in (D) are pooled from two independent experiments with n = 5/group, while data in (F) and (G) are representative from two independent experiments with n = 5/group. Data were analyzed using two-tailed unpaired Student's t test; ns, not significant; $^{**}p < 0.01$.

2020; Kastenmuller et al., 2012). To test whether this pro-inflammatory cytokine was involved in the recruitment of neutrophils, we injected an anti-IL-1β antibody 16 h before infection (Figure 5C). IL-1β ELISA on ear protein lysates revealed a proper blockade as compared with IgG controls (Figure S6A). Flow cytometry analysis of dLNs showed no difference in the number of recruited neutrophils (Figure 5D), indicating that IL-1β is not contributing to the influx of these granulocytes early after *L. mexicana* dermal infection.

SCS macrophages have been shown to be the cell source of the cues to which neutrophils respond in dLNs in several experimental models (Kastenmuller et al., 2012; Moran et al., 2019;

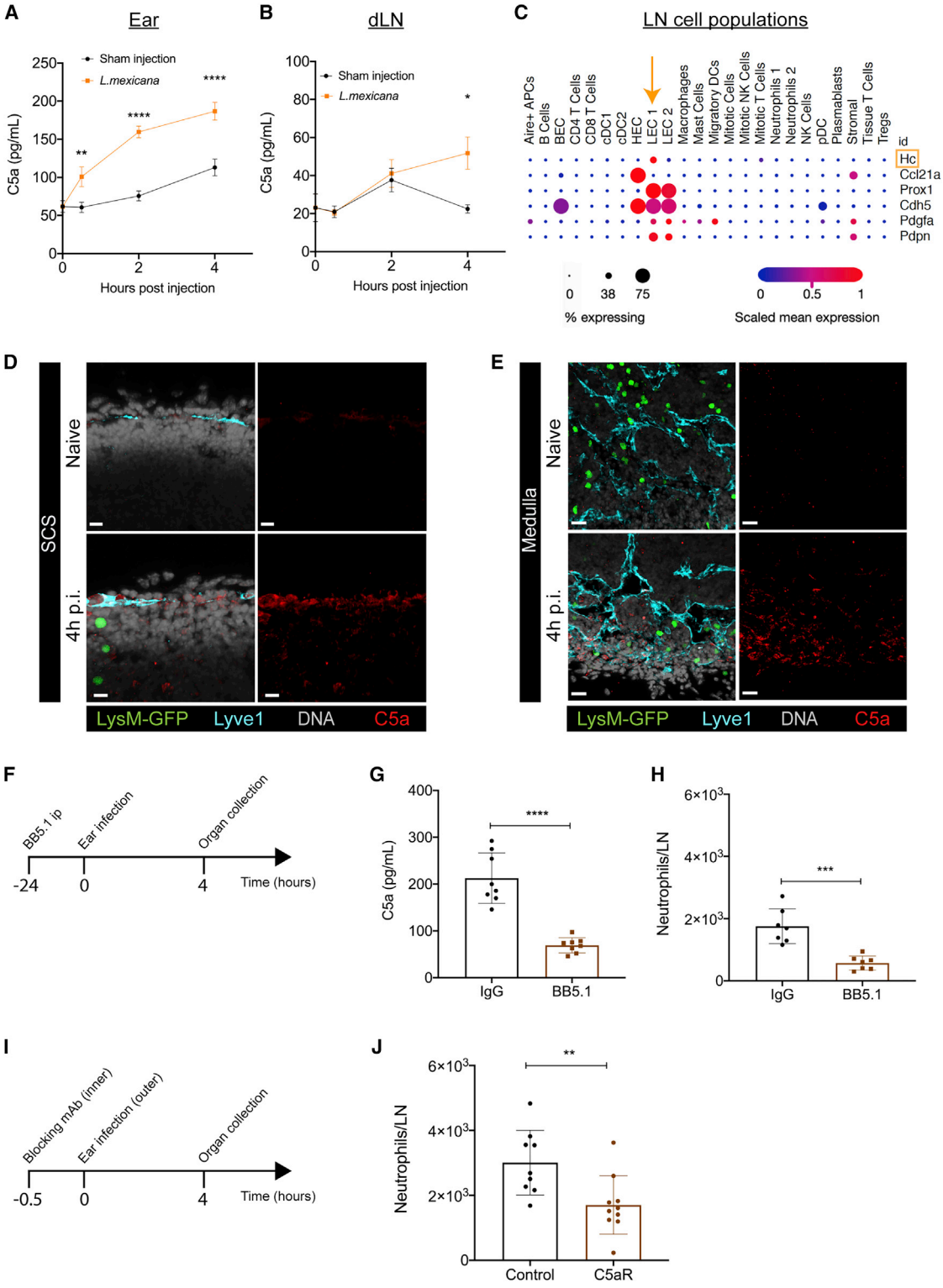

Figure 6. C5a promotes recruitment of neutrophils to dLNs in response to *L. mexicana* dermal infection

(A) C5a levels in ear protein lysates of naive, sham-injected, or infected mice 30 min, 2 and 4 h p.i.

(B) C5a levels in dLN protein lysates from naive, vehicle-injected, or infected mice 30 min, 2 and 4 h p.i.

(C) C5 is expressed in a subset of LN LECs. Single-cell RNA-seq showing different cell subsets of a naive murine LNs. Dotplot shows restricted Hc expression in the LEC1 group. Expression of the other genes confirms the purity of the endothelial cells: high endothelial cells (HECs) (from HEVs), Ccl21a^{+}Cdh5^{+}; blood

(legend continued on next page)

Sagoo et al., 2016). To assess if, in our model, they were involved in neutrophil recruitment, we delivered clodronate or PBS liposomes to the dLNs 7 and 5 days before infection to deplete macrophages (Figure 5E). To diminish the damage created by the injection we injected the liposomes in the inner side of the ear. We first corroborated, by injecting FITC-labeled dextran, that both the inner and outer side of the ear drain to the same LN (Figure S5B). Despite depletion of both SCS and medullary macrophages (Figure 5F), we did not observe a reduction of dLN neutrophils (Figure 5G). Instead, more neutrophils were present, indicating that early neutrophil recruitment to dLNs does not rely on LN macrophages during dermal *L. mexicana* infection.

Together, these data indicate that the neutrophil influx in the dLNs does not respond to IL-1β, nor to any macrophage-secreted molecule in the context of early *L. mexicana* infection.

Neutrophils are driven to the dLNs by the anaphylatoxin C5a

To identify the cues attracting neutrophils into the dLNs we first analyzed the chemokines produced by naive, sham-injected and infected dLNs 4 h p.i. using chemokine protein arrays. We were not able to detect any of the cytokines with the strongest neutrophil chemotactic activity, such as KC, LIX, or MIP-2 (Figure S7A). The CCL22 and MIP-1 γ chemokines displaying mild neutrophil chemotactic activity were detected but there was no difference compared with sham injection (Figures S7A and S7B).

C5a, the breakdown product of the C5 complement protein, displays strong chemotactic activity for neutrophils in the context of acute bacterial infection and chronic inflammatory diseases, such as arthritis (Bogoslowski et al., 2018; Miyabe et al., 2017). Furthermore, as an end-target molecule, neutrophils prioritize it over other molecules (Foxman et al., 1997; Metzemaekers et al., 2020). Therefore, we monitored C5a levels in the dLNs and ear by ELISA during the first 4 h after *L. mexicana* infection. At the infection site, the levels of C5a rapidly increased, with a 2-fold increase already observed 30 min after parasite inoculation. C5a levels continued to increase until reaching 187.6 pg/mL at 4 h p.i. (Figure 6A). In the dLNs, the levels of C5a were significantly higher than after sham injection 4 h p.i. (51.08 pg/mL), a timing that coincides with the peak of neutrophils observed in this organ (Figures 6B and 1A). The production of C5, as with most of the other complement proteins, primarily happens in the liver (Pontoglio et al., 2001; Ramadori et al., 1984). Nonetheless, there is also extrahepatic production of some of the complement components (Li et al., 2007). To explore if C5 was expressed in the dLNs, we analyzed a recent single-cell RNA-seq database of naive LNs (Huang et al., 2021). Dotplot analysis of the different LN cell populations revealed that *Hc* (C5) was expressed in lymphatic endothelial cells (LECs), specifically subset LEC1 (Figure 6C).

To confirm this observation at the protein level, we performed immunofluorescence staining on dLNs of LysM-GFP mice and stained for C5a, together with Lyve1 as an LEC marker. We found expression of C5a predominantly in the SCS, detected on the bottom layer of LECs (so-called floor LECs) (Petrova and Koh, 2020; Xiang et al., 2020). Furthermore, C5a was also present at the medullary site, also associated with Lyve1$^+$ cells (Figure 6D). Four hours p.i. C5a was more intensely detected at the medulla in association with the lymphatic endothelium. Of note, we also detected C5a at the SCS with the same pattern than that observed in the naive situation, but with a stronger signal (Figure 6E).

To test if neutrophil influx to the dLNs was driven by C5a in response *L. mexicana* infection, we performed *in vivo* blocking experiments using the BB5.1 mAb (Figure 6F). Blocking was efficient, as demonstrated by reduced C5a levels in the infected ear (Figure 6G). Most importantly, the number of neutrophils was significantly reduced upon C5 blockade as compared with the IgG group (Figure 6H), indicating that C5a is responsible for the recruitment of neutrophils to the dLNs. We also observed a significant reduction in the number of neutrophils in the dLNs upon blockade of C5aR1 using the B122 mAb (Figures 6I and 6F), which further highlights the central role of C5a signaling in neutrophil recruitment to the dLNs.

Altogether, our data indicate that neutrophils, in response to *L. mexicana* infection, migrate to the dLNs by the C5a-C5aR1 axis.

DISCUSSION

Neutrophils are increasingly recognized not only as mere frontline soldiers, but also as important players that influence the immune response during infections and cancer (Hedrick and Malanchi, 2021; Nicolas-Avila et al., 2017). However, their role in dLNs is controversial and the mechanisms by which neutrophils enter the dLNs are not fully characterized and seem heterogeneous. This study provides a mechanistic insight of neutrophil recruitment and extravasation into the dLNs tailored to the intracellular pathogen *L. mexicana*. We show that, upon dermal infection, there is a transient neutrophil recruitment to the dLNs. Despite rapid recruitment of neutrophils to the infected

endothelial cells (BECs), Cdh5$^+$; lymphatic endothelial cells (LECs), Prox1$^+$Cdh5$^+$Pdpn$^+$. Data were generated from Huang et al. (2021) using the Single Cell Portal.

(D–E) C5a protein localization in naive and infected dLNs. Immunofluorescence staining for C5a (red), Lyve1 (cyan), LysM-GFP (green), and DNA (gray). (D) Staining in the SCS area; (E) focus on the medulla. Scale bar, 20 μm.

(F) Experimental design for C5a-blocking experiments.

(G) C5a-blocking efficacy using the BB5.1 antibody was checked by ELISA in ear protein lysates from BB5.1- or IgG-treated mice 4 h after *L. mexicana* infection i.d.

(H) Absolute neutrophil numbers observed in dLNs of *L. mexicana* 4 h p.i., as analyzed by flow cytometry after BB5.1 blocking treatments and IgG controls.

(I) Experimental design for the C5aR1 blocking experiments.

(J) The number of dLN neutrophils was assessed by flow cytometry after injection of mAb against C5aR1 and control mAb treatments. Data in (A) and (B) are pooled of two independent experiments, with n = 4/group/time point. The data were analyzed using a mixed-effect analysis with Sydak's multiple comparison test. Data in (G) and (F) are pooled of two independent experiments with n = 4/group and were analyzed using two-tailed unpaired Student's t test. Data on (F) are a pool of two independent experiments with n = 5/group and were analyzed using two-tailed unpaired Student's t test; $^{**}p < 0.01$, $^{***}p < 0.001$, $^{****}p < 0.0001$.

ear, the majority of dLN neutrophils do not arrive from the infection site through lymphatic vessels. Instead, they enter the dLNs through HEVs guided to the anaphylatoxin C5a. We further show that this is an integrin and L-selectin-dependent process.

The infiltration of neutrophils in an infected tissue is a very fast process after infection with many types of pathogens, such as bacteria, virus, fungi, and parasites (Abadie et al., 2005; Abtin et al., 2014; Bouchery et al., 2020; Dey et al., 2018; Hurrell et al., 2015; Kirsebom et al., 2019; Regli et al., 2020; Swidergall et al., 2019; Tacchini-Cottier et al., 2000). However, the mechanisms of infiltration of these cells in LNs draining the affected area was only investigated recently (Bogoslowski et al., 2018, 2020; Hampton et al., 2015; Hampton and Chtanova, 2016). We provide an exhaustive kinetic of neutrophil infiltration in dLNs during the first 24 h of *L. mexicana* infection and show that neutrophils transiently peaked at 4 h p.i. and then returned to their basal levels. This transient rapid neutrophil recruitment in dLNs was also shown to be similar in the context of a subcutaneous CFA immunization, and use killed *S. aureus* infection (Hampton et al., 2015; Kamenyeva et al., 2015; Yang and Unanue, 2013). Nonetheless, when using a live *S. aureus* strain neutrophils persisted up to 48 h p.i. (Kamenyeva et al., 2015). This differential recruitment seems to indicate that there are stimuli-adapted neutrophilic responses in dLNs in addition to the infected site.

By comparing *S. aureus* bioparticles with *L. mexicana* infection we show that the parasite induced a lower neutrophilic response than that observed after injection with *S. aureus* bioparticles, more specially so in the dLNs. The source of these differences may come from several factors. Both pathogens differ in size, and this may have an impact on their dissemination in the dLNs. *S. aureus* is around 1 μm (Monteiro et al., 2015), which coincides with the reported maximum size of the pores from the LEC floor layer in the SCS (Forkert et al., 1977; van Ewijk et al., 1988). On the other hand, the *L. mexicana* promastigote is around 6 to 15 μm, considering or not the flagellum (Wheeler et al., 2011). Therefore, in the case of *L. mexicana* infection this could lead to a more restrained pathogen distribution in the dLNs, which eventually may be translated into a lower neutrophilic response.

The nature of each pathogen may also be important to explain this response. While *S. aureus* is an extracellular pathogen, *Leishmania* is an obligate intracellular microorganism and therefore the alert signals generated by the latter are probably less pronounced or silenced, resulting in less neutrophil recruitment. This phenomenon was already observed in the context of extracellular (*Pseudomonas aeruginosa*) versus intracellular bacteria (*Salmonella typhimurium*) (Kastenmuller et al., 2012).

The route used by neutrophils to reach the dLNs is still a subject of debate. Following *S. aureus* bioparticle injection, Hampton et al. state that neutrophils were primarily directed to the dLNs via lymphatics. However, only relatively infrequent intralymphatic neutrophils (<1% of total neutrophils) were detected and neutrophil recruitment via HEV was not analyzed (Hampton et al., 2015). Other reports showed neutrophil trafficking through blood vessels, via HEVs, in response to a methicillin-resistant *S. aureus* strain (Bogoslowski et al., 2018; Kamenyeva et al., 2015). Recently, using another methicillin-resistant *S. aureus* strain, little lymphatic migration was reported, in addition to a decrease in dLN neutrophils after i.p. injection of anti-L-selectin mAb, indicating neutrophil entry via HEV (Ozcan et al., 2022). Following infection with *Toxoplasma gondii*, another intracellular protozoan parasite, neutrophils were mostly found in the SCS of the dLNs, suggesting possible neutrophil entry via lymphatics (Chtanova et al., 2008). In our cell-tracking experiments, using Kikume mice as well as 2P-IVM studies performed on the Prox1-mOrange/LysM-GFP BM chimeras, we demonstrate that neutrophils, in response to both *L. mexicana* infection and *S. aureus* bioparticles, arrive to the dLNs mostly from the bloodstream and not from the infection site. Furthermore, neutrophils utilize HEVs to extravasate into the dLN parenchyma in response to *L. mexicana* dermal infection. In addition, the nearly complete absence of migration via lymphatics after infection with *L. mexicana* can also be explained by blocking mechanisms originating from the parasite itself, as shown by our transwell experiment results. In this line, *L. mexicana* was previously shown to impair dendritic cell migration to dLNs (Hsu and Scott, 2007; Hurrell et al., 2015; Petritus et al., 2012). Altogether, our data and these studies show that the magnitude of neutrophil response differs depending on the pathogenic threat. In addition, neutrophils can enter dLNs via lymphatics and HEV, but the main route of entry, quantitatively speaking, appears to be via HEVs.

Neutrophil's motion is key to performing their functions. In this sense, we observed that, in the ear parenchyma, neutrophils moved at a slower speed than those observed in the dLNs. This may reflect an attempt to limit the infection of *L. mexicana*, since neutrophil arrest has been recently shown to be critical for containment of *P. aeruginosa* (Kienle et al., 2021). However, as *L. mexicana* has been shown to suppress neutrophil microbicidal functions (Hurrell et al., 2015) this process would be deleterious for the host.

Neutrophil extravasation cascade has been elegantly established for neutrophils by 2P-IVM using the cremaster model (Girbl et al., 2018; Hickey and Kubes, 2009; Proebstl et al., 2012; Woodfin et al., 2011). Nevertheless, each vascular bed acquires organ-specific features to meet the functional demands and thus extrapolation of the molecular events from one organ to another might be farfetched (Augustin and Koh, 2017; Maas et al., 2018). Following infection with *L. mexicana*, neutrophils extravasate at the infection site following the "classical" cascade. Indeed, L-selectin and PSGL1 are key in their exit from the dermal vasculature, as was shown previously in the cremaster model (Stadtmann et al., 2013). In contrast, in the dLNs, L-selectin but not PSGL-1 was important for neutrophil entry into the parenchyma. The importance of L-selectin in monocyte recruitment was similarly reported in the context of *L. major* infection (Leon and Ardavin, 2008). Interestingly, in the context of *S. aureus* infection, neutrophils required both L-selectin and PSGL-1 to enter the dLNs (Bogoslowski et al., 2018), indicating pathogen-dependent modes of trafficking.

The engagement of selectins between the neutrophils and the endothelium leads to neutrophil integrin conformational changes that are then responsible for their slow rolling and arrest (Langereis, 2013). Neutrophils express several integrins: LFA-1 (CD11a), Mac1 (CD11b), and VLA-4 (CD49d) (Werr et al.,

1998). These three have been shown, using different experimental models, to be implicated in neutrophil extravasation in different organs (Li et al., 2012; Neumann et al., 2015; Volmering et al., 2016). Here, we show that, in response to *L. mexicana* infection, integrins are needed to enter the LN parenchyma, yet blockade of a single integrin was not able to impair neutrophil recruitment to the dLNs, suggesting compensatory mechanisms taking place in this organ. In contrast, LFA-1 and Mac1 were required for neutrophil extravasation to the infection site.

Neutrophils are attracted to, and able to respond to, many different signals, such as formyl peptides (e.g., fMLP), chemotactic lipids (e.g., LTB_4), and complement anaphylatoxins and chemokines (Metzemaekers et al., 2020). From the last category, CXCL1 (KC), CXCL5 (LIX), or CXCL2 (MIP-2) are classical neutrophil chemokines that were shown to attract neutrophils to visceral sites, such as the peritoneal cavity (De Filippo et al., 2008; Jackson-Jones et al., 2020; Song et al., 2013), as well as to the skin; for instance, to the site of *L. major* infection (Muller et al., 2001; Ronet et al., 2019). Nonetheless, their presence in dLNs was not assessed in these studies. We were unable to detect such chemokines in dLNs during the early hours after infection in our model. IL-1β had also been involved in the recruitment of neutrophils to dLNs in response to bacteria and viruses (Kastenmuller et al., 2012). We observe major expression of pro and mature IL-1β in macrophages, but IL-1β depletion did not impact the influx of neutrophils in dLNs in response to this protozoan parasite, indicating that IL-1β does not play a role in neutrophil influx to the dLNs in this model at this stage of infection. Again, this may be because of the fact that viruses and bacteria may become more numerous and spread to the SCS and target SCS macrophages, which then unleash such a response. Here, we show that C5a is behind this new recruitment, since impairing the cleavage of C5 by means of the monoclonal BB5.1 antibody or blocking C5aR1 resulted in a significant decrease of neutrophils. The recruitment of neutrophils to dLNs via C5aR1 was already reported in the context of *S. aureus* infection by Bogoslowski et al. (2018); however, in that study they reported a complete abolishment of neutrophil presence in the dLNs upon C5aR1 blockade treatment. This difference may reside in the nature of the model used.

We further show that LECs in the dLNs produce C5, which is prominent in those from the floor SCS and the medulla. This property of C5 production by LECs seems to be LN-specific as dermal LECs do not express it, at least at the mRNA level (Berendam et al., 2019; Gonzalez-Loyola et al., 2021). C5 and/or C5a may also reach the dLNs by plasma leakage and enter via lymphatic drainage from the infection site. Whether systemic or LN-LEC-derived C5 is specifically behind the neutrophil recruitment is still uncertain. Mice with conditional C5 inactivation in LECs would be invaluable to address this question.

In summary, our work details mechanistically how neutrophils are recruited to dLNs at the onset of cutaneous leishmaniasis. By means of HEVs, neutrophils reach the dLNs independently of integrins and, relying on L-selectin, are guided toward C5a. We further show that C5 is produced locally in the LNs by SCS floor and medullary LECs. This C5 production could represent a more general mechanism by which the LNs may rapidly recruit neutrophils following pathogen infections.

Limitations of the study

Our study provides a comprehensive understanding of the mechanisms involved in neutrophil migration to the lymph node draining the infection with the protozoan parasite *L. mexicana*. There are several limitations to our study. First, we show that L-selectin is essential in the recruitment of neutrophils to the draining lymph node; however, downstream molecules are also likely involved, and these remain to be identified. Second, needle injection of a high dose of parasites is needed to mimic the early neutrophil recruitment observed in the host dermis following the blood meal of infected sand flies. However, during a natural infection, the sand fly deposits significantly fewer parasites, together with vector and parasite-derived factors. It will be important to demonstrate in future experiments that similar mechanisms of neutrophil migration to the draining lymph node take place following natural infection. Finally, more than 20 *Leishmania* spp. have been reported to infect humans with distinct pathology outcomes. It would be important to translate our results to infection with other *Leishmania* sp. These will be future research areas stemming out from this initial study.

STAR★METHODS

Detailed methods are provided in the online version of this paper and include the following:

- KEY RESOURCES TABLE
- RESOURCE AVAILABILITY
  - Lead contact
  - Materials availability
  - Data and code availability
- EXPERIMENTAL MODEL AND SUBJETS DETAILS
  - Animal models
  - Bone marrow chimeras
  - Cell culture
- METHOD DETAILS
  - *In vivo* injections and treatments
  - Flow cytometry and Imaging flow cytometry
  - Ear whole mount staining
  - LN immunofluorescence
  - Two-photon intravital microscopy (2P-IVM)
  - *In vitro* transendothelial lymphatic migration
  - Tissue protein preparation
  - ELISA and protein arrays
- QUANTIFICATION AND STATISTICAL ANALYSIS
  - Image analysis and quantification
  - Quantification and statistical analysis
  - Public dataset analysis: Murine LN single cell RNA-seq

SUPPLEMENTAL INFORMATION

Supplemental information can be found online at https://doi.org/10.1016/j.celrep.2022.110777.

ACKNOWLEDGMENTS

We thank Yazmin Hauyon-La Torre, Maeva Delacrétaz, Florence Prével, and Stéphanie Favre for technical assistance. We are grateful to Friedmann Kiefer for providing the Prox1-mOrange mice. We thank Benjamin Hurrell and Esther

Bovay for their initial contribution to the project. We also thank Jens Stein for providing the labeled MECA79 antibody, the technical platform for 2P-IVM, and discussions. The Mouse Pathology Facility, Flow Cytometry Facility (Francisco Sala de Oyanguren), Cellular Imaging Facility (CIF), and the *In vivo* Imaging Facility (Alexandre Bénéchet) of UNIL are also acknowledged. Funding: This work was supported by the Swiss National Science Foundation Project Grant (310030_18475/1) to F.T.-C. L.F.-C. was supported by CAPES-PrInt UFRJ, a CAPES Foundation International Scholarship, Ministry of Education, Brazil.

AUTHOR CONTRIBUTIONS

B.P.-L. and F.T.-C. conceived and designed the research, interpreted the data, and drafted the manuscript. B.P.L., C.N., K.P., E.G., J.A., L.F.-C., and A.J.M. conducted the experiments, acquired and analyzed the data. A.J.M. and T.V.P. provided materials and intellectual input and interpreted the data. All authors read, commented on, and approved the manuscript.

DECLARATION OF INTERESTS

The authors declare no competing interests.

Received: October 21, 2021
Revised: February 24, 2022
Accepted: April 11, 2022
Published: May 3, 2022

REFERENCES

Aarts, C.E.M., Hiemstra, I.H., Tool, A.T.J., van den Berg, T.K., Mul, E., van Bruggen, R., and Kuijpers, T.W. (2019). Neutrophils as suppressors of T cell proliferation: does age matter? Front. Immunol. *10*, 2144. https://doi.org/10.3389/fimmu.2019.02144.

Abadie, V., Badell, E., Douillard, P., Ensergueix, D., Leenen, P.J., Tanguy, M., Fiette, L., Saeland, S., Gicquel, B., and Winter, N. (2005). Neutrophils rapidly migrate via lymphatics after Mycobacterium bovis BCG intradermal vaccination and shuttle live bacilli to the draining lymph nodes. Blood *106*, 1843–1850. https://doi.org/10.1182/blood-2005-03-1281.

Abtin, A., Jain, R., Mitchell, A.J., Roediger, B., Brzoska, A.J., Tikoo, S., Cheng, Q., Ng, L.G., Cavanagh, L.L., von Andrian, U.H., et al. (2014). Perivascular macrophages mediate neutrophil recruitment during bacterial skin infection. Nat. Immunol. *15*, 45–53. https://doi.org/10.1038/ni.2769.

Augustin, H.G., and Koh, G.Y. (2017). Organotypic vasculature: from descriptive heterogeneity to functional pathophysiology. Science *357*, eaal2379. https://doi.org/10.1126/science.aal2379.

Bai, Z., Cai, L., Umemoto, E., Takeda, A., Tohya, K., Komai, Y., Veeraveedu, P.T., Hata, E., Sugiura, Y., Kubo, A., et al. (2013). Constitutive lymphocyte transmigration across the basal lamina of high endothelial venules is regulated by the autotaxin/lysophosphatidic acid axis. J. Immunol. *190*, 2036–2048. https://doi.org/10.4049/jimmunol.1202025.

Beauvillain, C., Delneste, Y., Scotet, M., Peres, A., Gascan, H., Guermonprez, P., Barnaba, V., and Jeannin, P. (2007). Neutrophils efficiently cross-prime naive T cells in vivo. Blood *110*, 2965–2973. https://doi.org/10.1182/blood-2006-12-063826.

Berendam, S.J., Koeppel, A.F., Godfrey, N.R., Rouhani, S.J., Woods, A.N., Rodriguez, A.B., Peske, J.D., Cummings, K.L., Turner, S.D., and Engelhard, V.H. (2019). Comparative transcriptomic analysis identifies a range of immunologically related functional elaborations of lymph node associated lymphatic and blood endothelial cells. Front. Immunol. *10*, 816. https://doi.org/10.3389/fimmu.2019.00816.

Blanchard, L., and Girard, J.P. (2021). High endothelial venules (HEVs) in immunity, inflammation and cancer. Angiogenesis *24*, 719–753. https://doi.org/10.1007/s10456-021-09792-8.

Bogoslowski, A., Butcher, E.C., and Kubes, P. (2018). Neutrophils recruited through high endothelial venules of the lymph nodes via PNAd intercept disseminating Staphylococcus aureus. Proc. Natl. Acad. Sci. U S A. *115*, 2449–2454. https://doi.org/10.1073/pnas.1715756115.

Bogoslowski, A., Wijeyesinghe, S., Lee, W.Y., Chen, C.S., Alanani, S., Jenne, C., Steeber, D.A., Scheiermann, C., Butcher, E.C., Masopust, D., and Kubes, P. (2020). Neutrophils recirculate through lymph nodes to survey tissues for pathogens. J. Immunol. *204*, 2552–2561. https://doi.org/10.4049/jimmunol.2000022.

Bouchery, T., Moyat, M., Sotillo, J., Silverstein, S., Volpe, B., Coakley, G., Tsourouktsoglou, T.D., Becker, L., Shah, K., Kulagin, M., et al. (2020). Hookworms evade host immunity by secreting a deoxyribonuclease to degrade neutrophil extracellular traps. Cell. Host. Microbe. *27*, 277–289.e6. https://doi.org/10.1016/j.chom.2020.01.011.

Brulois, K., Rajaraman, A., Szade, A., Nordling, S., Bogoslowski, A., Dermadi, D., Rahman, M., Kiefel, H., O'Hara, E., Koning, J.J., et al. (2020). A molecular map of murine lymph node blood vascular endothelium at single cell resolution. Nat. Commun. *11*, 3798. https://doi.org/10.1038/s41467-020-17291-5.

Burn, G.L., Foti, A., Marsman, G., Patel, D.F., and Zychlinsky, A. (2021). The neutrophil. Immunity *54*, 1377–1391. https://doi.org/10.1016/j.immuni.2021.06.006.

Casanova-Acebes, M., Nicolas-Avila, J.A., Li, J.L., Garcia-Silva, S., Balachander, A., Rubio-Ponce, A., Weiss, L.A., Adrover, J.M., Burrows, K., N, A.G., et al. (2018). Neutrophils instruct homeostatic and pathological states in naive tissues. J. Exp. Med. *215*, 2778–2795. https://doi.org/10.1084/jem.20181468.

Chtanova, T., Schaeffer, M., Han, S.J., van Dooren, G.G., Nollmann, M., Herzmark, P., Chan, S.W., Satija, H., Camfield, K., Aaron, H., et al. (2008). Dynamics of neutrophil migration in lymph nodes during infection. Immunity *29*, 487–496. https://doi.org/10.1016/j.immuni.2008.07.012.

De Filippo, K., Henderson, R.B., Laschinger, M., and Hogg, N. (2008). Neutrophil chemokines KC and macrophage-inflammatory protein-2 are newly synthesized by tissue macrophages using distinct TLR signaling pathways. J. Immunol. *180*, 4308–4315. https://doi.org/10.4049/jimmunol.180.6.4308.

Deniset, J.F., Surewaard, B.G., Lee, W.Y., and Kubes, P. (2017). Splenic Ly6G(high) mature and Ly6G(int) immature neutrophils contribute to eradication of S. pneumoniae. J. Exp. Med. *214*, 1333–1350. https://doi.org/10.1084/jem.20161621.

Dey, R., Joshi, A.B., Oliveira, F., Pereira, L., Guimaraes-Costa, A.B., Serafim, T.D., de Castro, W., Coutinho-Abreu, I.V., Bhattacharya, P., Townsend, S., et al. (2018). Gut Microbes Egested during bites of infected sand flies augment severity of leishmaniasis via inflammasome-derived IL-1beta. Cell Host Microbe *23*, 134–143.e6. https://doi.org/10.1016/j.chom.2017.12.002.

Didelija, I.C., Mohammad, M.A., and Marini, J.C. (2017). Ablation of arginase II spares arginine and abolishes the arginine requirement for growth in male mice. J. Nutr. *147*, 1510–1516. https://doi.org/10.3945/jn.117.251249.

Faust, N., Varas, F., Kelly, L.M., Heck, S., and Graf, T. (2000). Insertion of enhanced green fluorescent protein into the lysozyme gene creates mice with green fluorescent granulocytes and macrophages. Blood *96*, 719–726.

Filipe-Santos, O., Pescher, P., Breart, B., Lippuner, C., Aebischer, T., Glaichenhaus, N., Spath, G.F., and Bousso, P. (2009). A dynamic map of antigen recognition by CD4 T cells at the site of leishmania major infection. Cell. Host Microbe. *6*, 23–33. https://doi.org/10.1016/j.chom.2009.04.014.

Forkert, P.G., Thliveris, J.A., and Bertalanffy, F.D. (1977). Structure of sinuses in the human lymph node. Cell. Tissue. Res. *183*, 115–130. https://doi.org/10.1007/BF00219996.

Foxman, E.F., Campbell, J.J., and Butcher, E.C. (1997). Multistep navigation and the combinatorial control of leukocyte chemotaxis. J. Cell. Biol. *139*, 1349–1360. https://doi.org/10.1083/jcb.139.5.1349.

Girbl, T., Lenn, T., Perez, L., Rolas, L., Barkaway, A., Thiriot, A., Del Fresno, C., Lynam, E., Hub, E., Thelen, M., et al. (2018). Distinct compartmentalization of the chemokines CXCL1 and CXCL2 and the atypical receptor ACKR1 determine discrete stages of neutrophil diapedesis. Immunity *49*, 1062–1076.e6. https://doi.org/10.1016/j.immuni.2018.09.018.

Gonzalez-Loyola, A., Bovay, E., Kim, J., Lozano, T.W., Sabine, A., Renevey, F., Arroz-Madeira, S., Rapin, A., Wypych, T.P., Rota, G., et al. (2021). FOXC2 controls adult lymphatic endothelial specialization, function, and gut lymphatic barrier preventing multiorgan failure. Sci. Adv. *7*, eabf4335. https://doi.org/10.1126/sciadv.abf4335.

Hagerling, R., Pollmann, C., Kremer, L., Andresen, V., and Kiefer, F. (2011). Intravital two-photon microscopy of lymphatic vessel development and function using a transgenic Prox1 promoter-directed mOrange2 reporter mouse. Biochem. Soc. Trans. *39*, 1674–1681. https://doi.org/10.1042/BST20110722.

Hampton, H.R., Bailey, J., Tomura, M., Brink, R., and Chtanova, T. (2015). Microbe-dependent lymphatic migration of neutrophils modulates lymphocyte proliferation in lymph nodes. Nat. Commun. *6*, 7139. https://doi.org/10.1038/ncomms8139.

Hampton, H.R., and Chtanova, T. (2016). The lymph node neutrophil. Semin. Immunol. *28*, 129–136. https://doi.org/10.1016/j.smim.2016.03.008.

Hampton, H.R., and Chtanova, T. (2019). Lymphatic migration of immune cells. Front. Immunol. *10*, 1168. https://doi.org/10.3389/fimmu.2019.01168.

Hedrick, C.C., and Malanchi, I. (2021). Neutrophils in cancer: heterogeneous and multifaceted. Nat. Rev. Immunol. *22*, 173–187. https://doi.org/10.1038/s41577-021-00571-6.

Heyde, S., Philipsen, L., Formaglio, P., Fu, Y., Baars, I., Hobbel, G., Kleinholz, C.L., Seiss, E.A., Stettin, J., Gintschel, P., et al. (2018). CD11c-expressing Ly6C+CCR2+ monocytes constitute a reservoir for efficient Leishmania proliferation and cell-to-cell transmission. PLoS Pathog. *14*, e1007374. https://doi.org/10.1371/journal.ppat.1007374.

Hickey, M.J., and Kubes, P. (2009). Intravascular immunity: the host-pathogen encounter in blood vessels. Nat. Rev. Immunol. *9*, 364–375. https://doi.org/10.1038/nri2532.

Hsu, A.C., and Scott, P. (2007). Leishmania mexicana infection induces impaired lymph node expansion and Th1 cell differentiation despite normal T cell proliferation. J. Immunol. *179*, 8200–8207. https://doi.org/10.4049/jimmunol.179.12.8200.

Huang, S., Ziegler, C.G.K., Austin, J., Mannoun, N., Vukovic, M., Ordovas-Montanes, J., Shalek, A.K., and von Andrian, U.H. (2021). Lymph nodes are innervated by a unique population of sensory neurons with immunomodulatory potential. Cell *184*, 441–459.e5. https://doi.org/10.1016/j.cell.2020.11.028.

Hurrell, B.P., Beaumann, M., Heyde, S., Regli, I.B., Muller, A.J., and Tacchini-Cottier, F. (2017). Frontline science: leishmania mexicana amastigotes can replicate within neutrophils. J. Leukoc. Biol. *102*, 1187–1198. https://doi.org/10.1189/jlb.4HI0417-158R.

Hurrell, B.P., Schuster, S., Grun, E., Coutaz, M., Williams, R.A., Held, W., Malissen, B., Malissen, M., Yousefi, S., Simon, H.U., et al. (2015). Rapid sequestration of leishmania mexicana by neutrophils contributes to the development of chronic lesion. PLoS Pathog. *11*, e1004929. https://doi.org/10.1371/journal.ppat.1004929.

Hyun, Y.M., and Hong, C.W. (2017). Deep insight into neutrophil trafficking in various organs. J. Leukoc. Biol. *102*, 617–629. https://doi.org/10.1189/jlb.1RU1216-521R.

Jackson-Jones, L.H., Smith, P., Portman, J.R., Magalhaes, M.S., Mylonas, K.J., Vermeren, M.M., Nixon, M., Henderson, B.E.P., Dobie, R., Vermeren, S., et al. (2020). Stromal cells covering omental fat-associated lymphoid clusters trigger formation of neutrophil aggregates to capture peritoneal contaminants. Immunity *52*, 700–715.e6. https://doi.org/10.1016/j.immuni.2020.03.011.

Kamenyeva, O., Boularan, C., Kabat, J., Cheung, G.Y., Cicala, C., Yeh, A.J., Chan, J.L., Periasamy, S., Otto, M., and Kehrl, J.H. (2015). Neutrophil recruitment to lymph nodes limits local humoral response to Staphylococcus aureus. PLoS Pathog. *11*, e1004827. https://doi.org/10.1371/journal.ppat.1004827.

Kastenmuller, W., Torabi-Parizi, P., Subramanian, N., Lammermann, T., and Germain, R.N. (2012). A spatially-organized multicellular innate immune response in lymph nodes limits systemic pathogen spread. Cell *150*, 1235–1248. https://doi.org/10.1016/j.cell.2012.07.021.

Kienle, K., Glaser, K.M., Eickhoff, S., Mihlan, M., Knopper, K., Reategui, E., Epple, M.W., Gunzer, M., Baumeister, R., Tarrant, T.K., et al. (2021). Neutrophils self-limit swarming to contain bacterial growth in vivo. Science *372*, eabe7729. https://doi.org/10.1126/science.abe7729.

Kirsebom, F.C.M., Kausar, F., Nuriev, R., Makris, S., and Johansson, C. (2019). Neutrophil recruitment and activation are differentially dependent on MyD88/TRIF and MAVS signaling during RSV infection. Mucosal Immunol. *12*, 1244–1255. https://doi.org/10.1038/s41385-019-0190-0.

Kolaczkowska, E., and Kubes, P. (2013). Neutrophil recruitment and function in health and inflammation. Nat. Rev. Immunol. *13*, 159–175. https://doi.org/10.1038/nri3399.

Langereis, J.D. (2013). Neutrophil integrin affinity regulation in adhesion, migration, and bacterial clearance. Cell Adh. Migr. *7*, 476–481. https://doi.org/10.4161/cam.27293.

Leliefeld, P.H., Koenderman, L., and Pillay, J. (2015). How neutrophils shape adaptive immune responses. Front. Immunol. *6*, 471. https://doi.org/10.3389/fimmu.2015.00471.

Leon, B., and Ardavin, C. (2008). Monocyte migration to inflamed skin and lymph nodes is differentially controlled by L-selectin and PSGL-1. Blood *111*, 3126–3130. https://doi.org/10.1182/blood-2007-07-100610.

Li, K., Sacks, S.H., and Zhou, W. (2007). The relative importance of local and systemic complement production in ischaemia, transplantation and other pathologies. Mol. Immunol. *44*, 3866–3874. https://doi.org/10.1016/j.molimm.2007.06.006.

Li, W., Nava, R.G., Bribriesco, A.C., Zinselmeyer, B.H., Spahn, J.H., Gelman, A.E., Krupnick, A.S., Miller, M.J., and Kreisel, D. (2012). Intravital 2-photon imaging of leukocyte trafficking in beating heart. J. Clin. Invest. *122*, 2499–2508. https://doi.org/10.1172/JCI62970.

Lok, L.S.C., Dennison, T.W., Mahbubani, K.M., Saeb-Parsy, K., Chilvers, E.R., and Clatworthy, M.R. (2019). Phenotypically distinct neutrophils patrol uninfected human and mouse lymph nodes. Proc. Natl. Acad. Sci. U S A. *116*, 19083–19089. https://doi.org/10.1073/pnas.1905054116.

Maas, S.L., Soehnlein, O., and Viola, J.R. (2018). Organ-specific mechanisms of transendothelial neutrophil migration in the lung, liver, kidney, and aorta. Front. Immunol. *9*, 2739. https://doi.org/10.3389/fimmu.2018.02739.

Metzemaekers, M., Gouwy, M., and Proost, P. (2020). Neutrophil chemoattractant receptors in health and disease: double-edged swords. Cell Mol. Immunol. *17*, 433–450. https://doi.org/10.1038/s41423-020-0412-0.

Miyabe, Y., Miyabe, C., Murooka, T.T., Kim, E.Y., Newton, G.A., Kim, N.D., Haribabu, B., Luscinskas, F.W., Mempel, T.R., and Luster, A.D. (2017). Complement C5a receptor is the key initiator of neutrophil adhesion igniting immune complex-induced arthritis. Sci. Immunol. *2*, eaaj2195. https://doi.org/10.1126/sciimmunol.aaj2195.

Monteiro, J.M., Fernandes, P.B., Vaz, F., Pereira, A.R., Tavares, A.C., Ferreira, M.T., Pereira, P.M., Veiga, H., Kuru, E., VanNieuwenhze, M.S., et al. (2015). Cell shape dynamics during the staphylococcal cell cycle. Nat. Commun. *6*, 8055. https://doi.org/10.1038/ncomms9055.

Moran, I., Grootveld, A.K., Nguyen, A., and Phan, T.G. (2019). Subcapsular sinus macrophages: the seat of innate and adaptive memory in murine lymph nodes. Trends. Immunol. *40*, 35–48. https://doi.org/10.1016/j.it.2018.11.004.

Muller, K., van Zandbergen, G., Hansen, B., Laufs, H., Jahnke, N., Solbach, W., and Laskay, T. (2001). Chemokines, natural killer cells and granulocytes in the early course of Leishmania major infection in mice. Med. Microbiol. Immunol. *190*, 73–76. https://doi.org/10.1007/s004300100084.

Neumann, J., Riek-Burchardt, M., Herz, J., Doeppner, T.R., Konig, R., Hutten, H., Etemire, E., Mann, L., Klingberg, A., Fischer, T., et al. (2015). Very-late-antigen-4 (VLA-4)-mediated brain invasion by neutrophils leads to interactions with microglia, increased ischemic injury and impaired behavior in experimental stroke. Acta Neuropathol. *129*, 259–277. https://doi.org/10.1007/s00401-014-1355-2.

Nicolas-Avila, J.A., Adrover, J.M., and Hidalgo, A. (2017). Neutrophils in homeostasis, immunity, and cancer. Immunity *46*, 15–28. https://doi.org/10.1016/j.immuni.2016.12.012.

Nowotschin, S., and Hadjantonakis, A.K. (2009). Use of KikGR a photoconvertible green-to-red fluorescent protein for cell labeling and lineage analysis in ES cells and mouse embryos. BMC. Dev. Biol. *9*, 49. https://doi.org/10.1186/1471-213X-9-49.

Ozcan, A., Collado-Diaz, V., Egholm, C., Tomura, M., Gunzer, M., Halin, C., Kolios, A.G.A., and Boyman, O. (2022). CCR7-guided neutrophil redirection to skin-draining lymph nodes regulates cutaneous inflammation and infection. Sci. Immunol. *7*, eabi9126. https://doi.org/10.1126/sciimmunol.abi9126.

Parsa, R., Lund, H., Georgoudaki, A.M., Zhang, X.M., Ortlieb Guerreiro-Cacais, A., Grommisch, D., Warnecke, A., Croxford, A.L., Jagodic, M., Becher, B., et al. (2016). BAFF-secreting neutrophils drive plasma cell responses during emergency granulopoiesis. J. Exp. Med. *213*, 1537–1553. https://doi.org/10.1084/jem.20150577.

Petritus, P.M., Manzoni-de-Almeida, D., Gimblet, C., Gonzalez Lombana, C., and Scott, P. (2012). Leishmania mexicana induces limited recruitment and activation of monocytes and monocyte-derived dendritic cells early during infection. PLoS Negl. Trop. Dis. *6*, e1858. https://doi.org/10.1371/journal.pntd.0001858.

Petrova, T.V., and Koh, G.Y. (2020). Biological functions of lymphatic vessels. Science *369*. https://doi.org/10.1126/science.aax4063.

Pontoglio, M., Pausa, M., Doyen, A., Viollet, B., Yaniv, M., and Tedesco, F. (2001). Hepatocyte nuclear factor 1alpha controls the expression of terminal complement genes. J. Exp. Med. *194*, 1683–1689. https://doi.org/10.1084/jem.194.11.1683.

Proebstl, D., Voisin, M.B., Woodfin, A., Whiteford, J., D'Acquisto, F., Jones, G.E., Rowe, D., and Nourshargh, S. (2012). Pericytes support neutrophil subendothelial cell crawling and breaching of venular walls in vivo. J. Exp. Med. *209*, 1219–1234. https://doi.org/10.1084/jem.20111622.

Puga, I., Cols, M., Barra, C.M., He, B., Cassis, L., Gentile, M., Comerma, L., Chorny, A., Shan, M., Xu, W., et al. (2011). B cell-helper neutrophils stimulate the diversification and production of immunoglobulin in the marginal zone of the spleen. Nat. Immunol. *13*, 170–180. https://doi.org/10.1038/ni.2194.

Ramadori, G., Rasokat, H., Burger, R., Meyer Zum Buschenfelde, K.H., and Bitter-Suermann, D. (1984). Quantitative determination of complement components produced by purified hepatocytes. Clin. Exp. Immunol. *55*, 189–196.

Regli, I.B., Passelli, K., Martinez-Salazar, B., Amore, J., Hurrell, B.P., Muller, A.J., and Tacchini-Cottier, F. (2020). TLR7 sensing by neutrophils is critical for the control of cutaneous leishmaniasis. Cell Rep. *31*, 107746. https://doi.org/10.1016/j.celrep.2020.107746.

Rigby, D.A., Ferguson, D.J., Johnson, L.A., and Jackson, D.G. (2015). Neutrophils rapidly transit inflamed lymphatic vessel endothelium via integrin-dependent proteolysis and lipoxin-induced junctional retraction. J. Leukoc. Biol. *98*, 897–912. https://doi.org/10.1189/jlb.1HI0415-149R.

Ronet, C., Passelli, K., Charmoy, M., Scarpellino, L., Myburgh, E., Hauyon La Torre, Y., Turco, S., Mottram, J.C., Fasel, N., Luther, S.A., et al. (2019). TLR2 signaling in skin nonhematopoietic cells induces early neutrophil recruitment in response to leishmania major infection. J. Invest Dermatol. *139*, 1318–1328. https://doi.org/10.1016/j.jid.2018.12.012.

Sagoo, P., Garcia, Z., Breart, B., Lemaitre, F., Michonneau, D., Albert, M.L., Levy, Y., and Bousso, P. (2016). In vivo imaging of inflammasome activation reveals a subcapsular macrophage burst response that mobilizes innate and adaptive immunity. Nat. Med. *22*, 64–71. https://doi.org/10.1038/nm.4016.

Schnoor, M., Vadillo, E., and Guerrero-Fonseca, I.M. (2021). The extravasation cascade revisited from a neutrophil perspective. Curr. Opin. Physiol. *19*, 119–128. https://doi.org/10.1016/j.cophys.2020.09.014.

Song, J., Wu, C., Zhang, X., and Sorokin, L.M. (2013). In vivo processing of CXCL5 (LIX) by matrix metalloproteinase (MMP)-2 and MMP-9 promotes early neutrophil recruitment in IL-1beta-induced peritonitis. J. Immunol. *190*, 401–410. https://doi.org/10.4049/jimmunol.1202286.

Sorensen, M., Lippuner, C., Kaiser, T., Misslitz, A., Aebischer, T., and Bumann, D. (2003). Rapidly maturing red fluorescent protein variants with strongly enhanced brightness in bacteria. FEBS Lett. *552*, 110–114. https://doi.org/10.1016/s0014-5793(03)00856-1.

Stadtmann, A., Germena, G., Block, H., Boras, M., Rossaint, J., Sundd, P., Lefort, C., Fisher, C.I., Buscher, K., Gelschefarth, B., et al. (2013). The PSGL-1-L-selectin signaling complex regulates neutrophil adhesion under flow. J. Exp. Med. *210*, 2171–2180. https://doi.org/10.1084/jem.20130664.

Stolp, B., Imle, A., Coelho, F.M., Hons, M., Gorina, R., Lyck, R., Stein, J.V., and Fackler, O.T. (2012). HIV-1 Nef interferes with T-lymphocyte circulation through confined environments in vivo. Proc. Natl. Acad. Sci. U S A. *109*, 18541–18546. https://doi.org/10.1073/pnas.1204322109.

Swidergall, M., Solis, N.V., Wang, Z., Phan, Q.T., Marshall, M.E., Lionakis, M.S., Pearlman, E., and Filler, S.G. (2019). EphA2 is a neutrophil receptor for candida albicans that stimulates antifungal activity during oropharyngeal infection. Cell. Rep. *28*, 423–433.e5. https://doi.org/10.1016/j.celrep.2019.06.020.

Tacchini-Cottier, F., Zweifel, C., Belkaid, Y., Mukankundiye, C., Vasei, M., Launois, P., Milon, G., and Louis, J.A. (2000). An immunomodulatory function for neutrophils during the induction of a CD4+ Th2 response in BALB/c mice infected with Leishmania major. J. Immunol. *165*, 2628–2636. https://doi.org/10.4049/jimmunol.165.5.2628.

Tecchio, C., and Cassatella, M.A. (2016). Neutrophil-derived chemokines on the road to immunity. Semin. Immunol. *28*, 119–128. https://doi.org/10.1016/j.smim.2016.04.003.

Tomura, M., Yoshida, N., Tanaka, J., Karasawa, S., Miwa, Y., Miyawaki, A., and Kanagawa, O. (2008). Monitoring cellular movement in vivo with photoconvertible fluorescence protein "Kaede" transgenic mice. Proc. Natl. Acad. Sci. U S A. *105*, 10871–10876. https://doi.org/10.1073/pnas.0802278105.

van Ewijk, W., Brekelmans, P.J., Jacobs, R., and Wisse, E. (1988). Lymphoid microenvironments in the thymus and lymph node. Scanning. Microsc. *2*, 2129–2140.

Vigl, B., Aebischer, D., Nitschke, M., Iolyeva, M., Rothlin, T., Antsiferova, O., and Halin, C. (2011). Tissue inflammation modulates gene expression of lymphatic endothelial cells and dendritic cell migration in a stimulus-dependent manner. Blood *118*, 205–215. https://doi.org/10.1182/blood-2010-12-326447.

Volmering, S., Block, H., Boras, M., Lowell, C.A., and Zarbock, A. (2016). The neutrophil Btk signalosome regulates integrin activation during sterile inflammation. Immunity *44*, 73–87. https://doi.org/10.1016/j.immuni.2015.11.011.

Werr, J., Xie, X., Hedqvist, P., Ruoslahti, E., and Lindbom, L. (1998). beta1 integrins are critically involved in neutrophil locomotion in extravascular tissue in vivo. J. Exp. Med. *187*, 2091–2096. https://doi.org/10.1084/jem.187.12.2091.

Wheeler, R.J., Gluenz, E., and Gull, K. (2011). The cell cycle of Leishmania: morphogenetic events and their implications for parasite biology. Mol. Microbiol. *79*, 647–662. https://doi.org/10.1111/j.1365-2958.2010.07479.x.

Woodfin, A., Voisin, M.B., Beyrau, M., Colom, B., Caille, D., Diapouli, F.M., Nash, G.B., Chavakis, T., Albelda, S.M., Rainger, G.E., et al. (2011). The junctional adhesion molecule JAM-C regulates polarized transendothelial migration of neutrophils in vivo. Nat. Immunol. *12*, 761–769. https://doi.org/10.1038/ni.2062.

Xiang, M., Grosso, R.A., Takeda, A., Pan, J., Bekkhus, T., Brulois, K., Dermadi, D., Nordling, S., Vanlandewijck, M., Jalkanen, S., et al. (2020). A single-cell transcriptional roadmap of the mouse and human lymph node lymphatic vasculature. Front. Cardiovasc. Med. *7*, 52. https://doi.org/10.3389/fcvm.2020.00052.

Yang, C.W., and Unanue, E.R. (2013). Neutrophils control the magnitude and spread of the immune response in a thromboxane A2-mediated process. J. Exp. Med. *210*, 375–387. https://doi.org/10.1084/jem.20122183.

STAR★METHODS

KEY RESOURCES TABLE

REAGENT or RESOURCE	SOURCE	IDENTIFIER
Antibodies		
Rabbit anti-mouse/human C5a	BiossAntibodies	Cat# bs-0324R, RRID:AB_10857063
Rabbit anti-RFP	Rockland	Cat# 600-401-379S, RRID:AB_11182807
Rat anti-mouse CD31, Clone: MEC13.3	BD Bioscience	Cat# 553370, RRID:AB_394816
Rat anti-mouse CD169, Clone: 3D6.112	Bio-Rad	Cat# MCA884GA, RRID:AB_324211
Goat anti-mouse IL-1β	R&D	Cat# AF-401-NA, RRID:AB_416684
Rabbit anti-mouse Lyve1	ReliaTech	Cat# 103-PA50, RRID:AB_2783787
Rat anti-mouse PNAd, Clone: MECA-79	BD Bioscience	Cat# 553863, RRID:AB_395099
Rat anti-mouse CD11b, Pacific Blue, Clone: M1/70	Invitrogen	Cat# 48-0112-80, RRID:AB_1582237
Rat anti-mouse Ly6G, APC-Cy7, Clone: 1A8	BioLegend	Cat# 127624, RRID:AB_10640819
Donkey anti rabbit Alexa Fluor-488	Life technologies	Cat# ab150073, RRID:AB_2636877
Donkey anti goat Alexa Fluor-488	Life technologies	Cat# A-11055, RRID:AB_2534102
Donkey anti rabbit Alexa Fluor-555	Life technologies	Cat# A32794, RRID:AB_2762834
Donkey anti rat Alexa Fluor-555	Life technologies	Cat# SA5-10027, RRID:AB_2556607
Donkey anti goat Alexa Fluor-647	Life technologies	Cat# ab150131, RRID:AB_2732857
Chicken anti rat Alexa Fluor-647	Life technologies	Cat# A-21472, RRID:AB_2535875
A.hamster anti-mouse/rat IL-1β, Clone: B122	BioXCell	Cat# BE0246, RRID:AB_2687727
Mouse anti-mouse C5, Clone: BB5.1	HycultBiotech	Cat# HM1073, RRID:AB_1212150
Rat anti-mouse C5aR1 (CD88), Clone: 20/70	BioLegend	Cat# 135815, RRID:AB_2819875
Rat anti-mouse L-selectin, Clone: Mel-14	BioXCell	Cat# BE0021, RRID:AB_1107665
Rat anti-mouse PSGL1, Clone: 4RA10	BioXCell	Cat# BE0186, RRID:AB_10950305
Rat anti-mouse LFA-1, Clone: M17/4	BioXCell	Cat# BE0006, RRID:AB_1107578
Rat anti-mouse/human Mac1, Clone: M1/70	BioXCell	Cat# BE0007, RRID:AB_1107582
Rat anti-mouse/human VLA4, Clone: PS/2	BioXCell	Cat# BE0071, RRID:AB_1107657
Mouse IgG control, Clone: MOPC-21	BioXCell	Cat# BE0083, RRID:AB_1107784
A.hamster IgG control	BioXCell	Cat# BE0091, RRID:AB_1107773
Rat IgG control, Clone: 2A3	BioXCell	Cat# BE0089, RRID:AB_1107769
Chemicals, peptides, and recombinant proteins		
CellTracker Orange CMRA Dye	Invitrogen	Cat#C34551
Hygromycin B	Roche	Cat#10843555001
Penicillin-Streptomycin-Neomycin	Gibco	Cat#31150-022
Fluoromount-G	eBioscience	Cat#00-4959-52
FITC-dextran (2000 kD)	Sigma	Cat#FD2000S
Collagenase D	Roche	Cat#11-088-866-001
Collagen I	Advanced Biomatrix	Cat#5005
Liberase TL	Roche	Cat#250850
Fibronectin	Millipore	Cat#FC010
Heparin	Sigma	Cat#H3149
Murine TNFα	ImmunoTools	Cat#12343014
DNase I	Roche	Cat#11-284-932-001
HEPES buffer	BioConcept AG	Cat#5-31F00-H
Ficoll	Sigma Aldrich	Cat#F5415
murine KC (CXCL1)	ImmunoTools	Cat#12343700
Fetal Bovine Serum	PAN-Biotech	Cat#P30-3306
DAPI	Sigma	Cat#D9542-10ML

(*Continued on next page*)

Continued

REAGENT or RESOURCE	SOURCE	IDENTIFIER
Critical commercial assays		
BCA protein quantification Kit	Thermofisher	Cat#23227
Neutrophil Isolation Kit mouse	Milteny Biotech	Cat#130-097-658
Mouse C5a ELISA kit	RayBiotech	Cat#ELM-CCC5a
Mouse IL-1β ELISA kit	Invitrogen	Cat#88-7013-88
Live/Dead Fixable Aqua Dead Cell Stain Kit	Invitrogen	Cat#L349577
Quantibody Mouse Chemokine Array Q1	RayBiotech	Cat#QAM-CHE-1-2
Deposited data		
Processed data, Seq-Well of LN-resident cells	Single Cell Portal	https://singlecell.broadinstitute.org/single_cell/study/SCP1186
Experimental models: Cell lines		
imLECs	Vigl et al., 2011	N/A
Experimental models: Organisms/strains		
Parasite: *Leishmania mexicana*	WHO	MYNC/BZ/62/M379
Parasite: *Leishmania mexicana DsRed*	Sorensen et al., 2003	N/A
Mouse: C57BL/6JOlaHsd	Envigo	RRID:MGI:5657800
Mouse: Lyz2$^{tm1.1Graf}$ (LysM-GFP)	Faust et al., 2000	RRID:MGI:2654931
Mouse: B6-Tg (Prox1::mOrange2)^{Fki} (Prox1-mOrange)	Hagerling et al., 2011	N/A
Mouse: Gt (ROSA)26Sor$^{tm2.1(CAG-kikGR)Kgwa}$ (Kikume)	Tomura et al., 2008	RRID:MGI:6477340
Software and algorithms		
FlowJo v10	FlowJo LLC.	RRID:SCR_008520
GraphPad PRISM 9	GraphPad Software	RRID:SCR_002798
Imaris	Bitplane	RRID:SCR_007370
FIJI	NIH	RRID:SCR_002285
Mapix	Innopsys	RRID:SCR_002723

RESOURCE AVAILABILITY

Lead contact

Further information and requests for resources and reagents should be directed to and will be fulfilled by the lead contact, Fabienne Tacchini-Cottier (fabienne.tacchini-cottier@unil.ch).

Materials availability

This study did not generate new unique reagents.

Data and code availability

- This paper analyzes existing, publicly available data. The accession number is listed in the key resources table.
- This paper does not report original code.
- Any additional information required to reanalyze the data reported in this paper is available from the lead contact upon request.

EXPERIMENTAL MODEL AND SUBJETS DETAILS

Animal models

Mice

C57BL/6 mice were purchased from Envigo (Cambridgeshire, United Kingdom). LysM-GFP, a gift from Prof. Sussan Nourshargh (Queen Mary, University of London) (Faust et al., 2000), Prox1-mOrange (Hagerling et al., 2011), a gift from Friedmann Kiefer, and Kikume mice, provided by Andreas J. Müller (Tomura et al., 2008) were all in C57BL/6 background. Mice were bred under pathogen-free conditions at the Epalinges Center. 6 to 12 weeks old females were used for all experiments. Animal experimental protocols were approved by the veterinary office regulations of the Canton of Vaud, Switzerland, under authorization 3476.d to FTC and performed in compliance with Swiss laws for animal protection, or by the Ethics Committee of the Office for Veterinary Affairs of the State of Saxony-Anhalt, Germany (permit license numbers 42502-2-1253 Uni MD, and 42502-2-1314 Uni MD) to AJM in accordance

with legislation of both the European Union (Council Directive 499 2010/63/EU) and the Federal Republic of Germany (according to § 8, Section 1 TierSchG, and TierSchVersV).

The goal of these studies was to demonstrate how neutrophils traffic into the dLN in response to *L. mexicana* infection. In all assays, sample size was determined on the basis of pilot experiments in our laboratory to allow us to get reliable data to perform statistical analyses and ensure reproducibility. Experiments were replicated in at least two to three independent experiments. The number of individual replicates for each experiment is indicated in the figure legends. To implement 3R guidelines we considered ears and dLNs as independent events. Animals were randomly assigned to different experimental groups.

Bone marrow chimeras

Prox1-mOrange mice were irradiated with a final 8.7 Gray (Gy) dose and reconstituted with LysM-GFP bone marrow. The recovered BM cells were intravenously transplanted into the tail vein as 10^6 cells in 150 ul of PBS. Mice were kept under antibiotics and anti-inflammatories in drinking water for 2 weeks. A cream was applied to the back of the mice for 3 consecutive days post-irradiation to avoid hair loss. Reconstitution was verified 6 weeks after transplantation by flow cytometry and/or histology.

Cell culture

Parasites

WT *L. mexicana* (WHO strain MYNC/BZ/62/M379) and *L. mexicana* DsRed (Sorensen et al., 2003), a gift from Prof. Tony Aebischer (Robert Koch-Institute, Berlin) were used. Parasites were cultured at 26°C in M199 medium (Gibco), supplemented with 10% foetal calf serum (FCS), 4% HEPES, and 2% PSN (Penicillin, Streptomycin and Neomycin, Bioconcept, Allschwill). Transgenic DsRed parasites were grown under the same conditions plus 50 μg/mL Hygromycin B (Sigma-Aldrich). Metacyclic parasites were selected by density centrifugation, as previously described (Hurrell et al., 2015).

Cell lines

imLECs (Vigl et al., 2011), a kind gift from Cornelia Halin (ETH, Zurich), were maintained in DMEM/F12 (Gibco), supplemented with 10% FBS, 1% P/S (Gibco), 10 μg /ml endothelial growth supplement (Sigma) and 56 μg/ml heparin (Sigma) at 37°C in a humidified 5% CO2 atmosphere.

METHOD DETAILS

In vivo injections and treatments

10^6 metacyclic parasites were injected into the ear dermis or footpad in 10 μl of endotoxin-free PBS. $2x10^7$ unlabelled *Staphylococcus aureus* bioparticles (Thermo Fisher) in 10 μL of PBS were injected into the ear dermis. For IL-1β and C5 blocking experiments mice were treated ip with 200 μg 16 hours or 250 μg 24 hours prior to infection, respectively. To block C5aR1 10 μl of the B122 antibody was injected i.d. 30 minutes before infection. For selectins and integrins blocking experiments 200 or 100 μg of blocking antibodies were delivered iv 1 hour before infection respectively. Appropriate Ig-matched antibodies were used as controls via the same route. For macrophage depletion experiments, clodronate liposomes (CLL) or PBS liposomes as control (Liposoma research, Amsterdam) were injected into the inner ear dermis 7 and 5 days before infection, to a final dose of 50 μg.

For neutrophil tracking experiments an M405 L3 High Power Diode (ThorLabs) in combination with a Collimator lens was used to photoconvert the ear tissue. For this, mice were anesthetized and the ears were placed in a distance from the collimating lens to the sample of 23 cm, resulting in an illumination intensity of 100mW/cm^2 (in total 143 mW in an area of 1.1 x 1,3 cm). The photoconversion was performed for 30 seconds on each side of the ear.

Flow cytometry and Imaging flow cytometry

Ears were collected at the indicated timepoints and processed to obtain a single cell suspension as previously described (Regli et al., 2020). Briefly, the two dermal layers were separated, homogenized and digested at 37°C for 2 hours in 0.2 mg/mL of liberase TL (Roche). Digested ears were further processed by using 40-μm filters (Falcon). Draining lymph nodes were recovered and digested in DMEM containing 2% Collagenase D and 0.4% DNase I for 15 minutes at 37°C, as delivered by needle puncture of the LN stroma, followed by homogenization. Blood was harvested by cardiac puncture and retained in 1% EDTA in PBS. Blood, bone marrow and spleen were treated with ACK buffer for erythrocyte lysis. Single cell suspensions were stained with the antibodies listed in the key resources table (KRT) diluted in the isolated supernatant of 2.4G2 hybridoma cells. Aqua Live/dead (Invitrogen) was used to gate on alive cells. Events were acquired with and LSR-Fortessa or LSR-SORP (BD Bioscience) and analyzed with FlowJo software (Tree StarA). To detect intracellular or surface-bound parasites, *L mexicana* was labelled with CMRA (Cell tracker™ Orange, Life technologies), while neutrophils were stained with Ly6G-APC (eBiosciences). Samples were analysed on an ImageStream cytometer (Amnis; Millipore Sigma, Billerica, MA, USA) at low speed and 60X magnification. An average of 15.000 events were acquired based on the brightfield. $DAPI^-$ living single cells were gated, followed by double positive cells ($Ly6G^+CMRA^+$). After selecting $CMRA^+$ spots, a mask was created based on the Ly6G staining and used for the identification of internalised versus externalised parasites by measuring the relative location of the $CMRA^+$ spot compared to the membrane staining of neutrophils. Data was analysed using the IDEAS software (version 6.2, Luminex).

Ear whole mount staining

Ears were harvested and fixed in 4% PFA overnight under gentle shaking. After PBS washing, ear leaflets were separated and pinned in an elastomere-coated well. Separated leaflets were blocked in blocking buffer (0.5% BSA-5% donkey serum-0.3% Triton X-100-01% Sodium azide-PBS) overnight at 4°C and stained with the primary antibodies previously diluted in blocking buffer overnight at 4°C under gentle agitation (see Key resources table). The following day, after washing, secondary antibodies diluted in blocking buffer were incubated overnight at 4°C under gentle agitation (see Key resources table). Following the washes, samples were mounted in Fluoromount-G with DAPI (Invitrogen). Images were acquired with an inverted confocal microscope Zeiss LSM 880 with Airyscan and processed in Imaris 9.0 (Bitplane) and FIJI softwares.

LN immunofluorescence

8 or 20-μm OCT cryosections were thawed for 30 minutes at room temperature, fixed for 10 minutes in 4% PFA and washed with 0.3% Triton X-100 in PBS. After 30 minutes in blocking buffer (0.5% BSA, 5% donkey serum, 0.3% Triton X-100, 0,1% NaN3), slides were incubated with primary antibody (see Key resources table) overnight at 4°C. The next day slides were washed with 0.3% Triton X-100 in PBS for 30 minutes and Alexa secondary antibodies 488/555/647 were added 1:500 in blocking buffer for 1 hour at RT. After that, slides were washed with 0.3% Triton X-100 in PBS for 30 minutes and mounted in Fluoromount-G, containing DAPI (Invitrogen).

For vibratome sections, LNs were fixed overnight at 4°C in 4% PFA, washed, and embedded in 4% (wt/vol) low-melting agarose (Sigma-Aldrich) in PBS. Then 100-μm sections were cut with a vibratome (Microm HM 650 V). Sections were blocked with 1% BSA for 1 h and stained for at least 3 days with the antibodies listed in the Key resources table. After PBS washing sections were incubated for another 3 days in secondary antibodies (see Key resources table).

Images were captured using a Zeiss LSM 880 with Airyscan or Leica SP5 TANDEM confocal microscopes and analyzed using Imaris and FIJI softwares. Tiled images were acquired using a motorized Zeiss time-lapse Axio Observer.Z1 with AxioVision Rel.4.7 software.

Two-photon intravital microscopy (2P-IVM)

Mice were anaesthetized with isofluorane during all the procedure. For ear imaging, the ear pinna was spread with the inner side on top on a custom-made stage heated to 37°C and processed as reported previously (Filipe-Santos et al., 2009). For LN imaging, popliteal lymph node was surgically exposed and prepared as reported previously (Stolp et al., 2012).

Intravital imaging was performed using a Trimscope II from LaVision BioTec (Miltenyi Biotec), equipped with two laser excitations lines. A titanium-sapphire (TiSA) laser pumping and an optical parameter oscillator (OPO) (Chameleon line, Coherent) were tuned to 820 nm and 1100 nm, respectively. Emitted fluorescence was sequentially split by 488, 635 nm and 565 nm long pass dichroic mirrors and filtered with 510/20 nm (GFP), 595/40 (Prox1mOrange) and 670/50 (far red dye). Four-dimensional full-scale images were analyzed using the Tracking and Colocalization modules of the Imaris Software (Bitplane, Zurich, Switzerland).

In vitro transendothelial lymphatic migration

imLECs were grown on the lower surface of 3-μm pore sized transwell inserts (Biofil), coated with 10 μg/ml Collagen I (Advanced Biomatrix) and 10 μg/ml fibronectin (Millipore). imLECs were then starved for 6 hours and stimulated with 10 ng/ml TNFα (ImmunoTools) for 12 hours.

Femora and tibia were collected, and bone marrow was obtained by centrifugation. Neutrophils were purified by positive magnetic-activated cell sorting (MACS) using Ly6G MicroBeads UltraPure isolation kit, according to manufacturer's instructions (MiltenyiBiotec). Neutrophil purity (>95%) was confirmed by cytospin preparation and flow cytometry. Neutrophils were then incubated with metacyclic parasites at an MOI of 1 for 2 hours. Not internalized, free parasites were removed by centrifugation and infected neutrophils were added to the upper surface of the transwell in 100 μl. When indicated, KC (final concentration: 0.1 μg /ml, ImmunoTools) was added to the bottom compartment. Cells that passed after 2 hours to the bottom compartment were then recovered and analyzed by flow cytometry.

Tissue protein preparation

Ear and dLNs were collected at the indicated time points, snap frozen in liquid nitrogen and homogenized in PBS using a magnetic bead and a tissue lyser (Qiagen). Protein was quantified using BCA assay.

ELISA and protein arrays

Mouse C5a (RayBiotech) and IL-1β (Invitrogen) ELISA kits, as well as Quantibody Mouse Chemokine Array (RayBiotech) were used according to the manufacturer's instructions. Slides from chemokine array were scanned using an Agilent scanner and data extraction was performed using RayBotech's specific GAL file on Mapix software.

QUANTIFICATION AND STATISTICAL ANALYSIS

Image analysis and quantification

To quantify neutrophils inside vessels by whole mount staining, a volume was generated with Imaris software based on CD31 or Lyve1 staining, for total vessels or lymphatic capillaries respectively. For collecting vessels, the volume of each collector was created

manually based on CD31 staining and morphology (faint CD31 staining and valve presence). Area of neutrophils contained in this volume was then divided by the area occupied by all neutrophils to obtain a percentage.

To quantify neutrophils in the different dLNs compartments tiled images were loaded into FIJI. Each compartment was manually defined based on DAPI and CD31 stainings and neutrophils or parasites contained in each compartment were then normalized to the total area of each corresponding zone.

Quantification and statistical analysis

p values were determined using GraphPad Prism version 8. Statistical difference between two groups were analyzed using t test, while differences among multiple groups were determines using ANOVA or a mixed-effect analysis with multiple comparisons. The tests used for each situation are specified in each figure's legend.

Public dataset analysis: Murine LN single cell RNA-seq

Murine steady-state inguinal LN single cell RNA-seq data was obtained from (Huang et al., 2021) and expression of selected genes was displayed in a dotplot for the identified cell populations with the help of the Single Cell Portal website (https://singlecell.broadinstitute.org/single_cell).